Article

Simulation of multiannual thermal profiles in deep Lake Geneva: A comparison of one-dimensional lake models

PERROUD, Marjorie, *et al*.

Abstract

In this study, we report on the ability of four one-dimensional lake models to simulate the water temperature profiles of Lake Geneva, the largest water body in Western Europe, over a 10-yr period from 1996 to 2005, using lake models driven by a common atmospheric forcing. These lake models have already demonstrated their capability of reproducing the temperature distribution in smaller lakes and include one eddy-diffusive lake model, the Hostetler model; a Lagrangian model, the one-dimensional Dynamic Reservoir Simulation Model ‘‘DYRESM''; a k–e turbulence model, ‘‘SIMSTRAT''; and one based on the concept of self-similarity (assumed shape) of the temperature–depth curve, the Freshwater Lake model ‘‘FLake.'' Only DYRESM and SIMSTRAT reproduce the variability of the water temperature profiles and seasonal thermocline satisfactorily. In layers in which thermocline variability is greatest, the temperature root mean square error is ,2uC and 3uC (at the time of highest stratification) for these models, respectively. It is possible to apply certain one-dimensional lake models that simulate the behavior of [...]

Reference

PERROUD, Marjorie, *et al*. Simulation of multiannual thermal profiles in deep Lake Geneva: A comparison of one-dimensional lake models. *Limnology and oceanography, methods*, 2009, vol. 54, no. 5, p. 1574-1594

Limnol. Oceanogr., 54(5), 2009, 1574–1594

Simulation of multiannual thermal profiles in deep Lake Geneva: A comparison of one-dimensional lake models

Marjorie Perroud,[a,*] Stéphane Goyette,[a] Andrey Martynov,[b] Martin Beniston,[a] and Orlane Anneville[c]

[a] Climatic Change and Climate Impacts (C³I), University of Geneva, Carouge, Geneva, Switzerland
[b] Canadian Regional Climate Modelling and Diagnostics (CRCMD) Network, University of Quebec in Montreal, Montreal, Quebec, Canada
[c] Orlane Anneville, French National Institute for Agricultural Research, INRA–Station d'Hydrobiologie Lacustre, Thonon-les-Bains Cedex, Haute-Savoie, France

Abstract

In this study, we report on the ability of four one-dimensional lake models to simulate the water temperature profiles of Lake Geneva, the largest water body in Western Europe, over a 10-yr period from 1996 to 2005, using lake models driven by a common atmospheric forcing. These lake models have already demonstrated their capability of reproducing the temperature distribution in smaller lakes and include one eddy-diffusive lake model, the Hostetler model; a Lagrangian model, the one-dimensional Dynamic Reservoir Simulation Model "DYRESM"; a k–ε turbulence model, "SIMSTRAT"; and one based on the concept of self-similarity (assumed shape) of the temperature–depth curve, the Freshwater Lake model "FLake." Only DYRESM and SIMSTRAT reproduce the variability of the water temperature profiles and seasonal thermocline satisfactorily. In layers in which thermocline variability is greatest, the temperature root mean square error is $<2^{\circ}$C and 3°C (at the time of highest stratification) for these models, respectively. It is possible to apply certain one-dimensional lake models that simulate the behavior of temperature to investigate the potential future warming of the water column in Lake Geneva. Importantly, the metalimnion boundary is successfully modeled, which represents an encouraging step toward demonstrating the feasibility of coupling biogeochemical modules, such as, for example, a phytoplanktonic model, to assess the possible biological responses within lakes to climate change.

Although peri-alpine lakes are generally renowned for their scenery, they also feature extensive biodiversity, support commercial fishing activities, and are reservoirs of drinking water for thousands of inhabitants. In Switzerland, around 20% of the domestic water supply comes from lakes (SVGW 2008). It is thus essential that the quality of these freshwater bodies be preserved. Many of the Swiss lakes were declared polluted after eutrophication in the early 1950s (e.g., Lake Geneva shared by France and Switzerland, Lake Constance shared by Germany and Switzerland, and the Swiss Lakes Neuchâtel, Biel, and Zug), and political efforts were undertaken over the following decades to decrease their phosphorus or nitrate loads (SAEFL 1994).

Since nutrient concentrations have decreased to values associated with an improved trophic status, these lakes now face changes associated with present and future climate. Some of the reported thermal effects of global warming include earlier onset of stratification, less frequent complete winter overturning in large lakes, stronger thermal gradients in the thermocline, shallower depths of the thermocline and an overall warming of the entire water column (King et al. 1997; McCormick and Fahnenstiel 1999; Peeters et al. 2002). Climate-induced changes of lake water temperatures and dynamics and the intensity of stratification disturb the functioning of aquatic ecosystems (Gerten and Adrian 2000; Anneville et al. 2002; Straile et al. 2003). In some cases, they also promote the development of toxic cyanobacteria (Jöhnk et al. 2008; Shatwell et al. 2008) and delay the recovery of lakes after eutrophication (Anneville et al. 2002, 2004). Under such conditions, the presence of such toxic algae in the aquatic ecosystems of a number of peri-alpine lakes [e.g., *Planktotrix rubescens* in Lake Geneva, Lake Bourget (Jacquet et al. 2005), Lake Zürich (Walsby and Schanz 2002), and Lake Pusiano (Legnani et al. 2005)] indicates that this problem should be investigated further. Predictions of the thermal evolution of lakes will help to assess changes in frequencies of toxic blooms that are likely to occur in some particular lakes.

Numerical investigations of the thermal evolution of a few peri-alpine lakes in a warmer climate, such as Lakes Constance and Zürich, have been reported in the literature, indicating significant changes in the long term (Peeters et al. 2002, 2007). However, Lake Geneva has never fully been studied to address this particular problem. Consequently, the main objective of this study is to simulate multiannual cycles of temperature profiles at a deep lacustrine station in Lake Geneva using one-dimensional (also referred to as single-column) numerical models.

The assumption behind the use of one-dimensional lake models is that vertical gradients of temperature and salinity are significantly larger than the horizontal ones. This assumption is valid if density stratification is present, external forces resulting from wind stress are weak, in- and outflows are not very significant, and other processes that could also generate horizontal gradients are negligible. The atmospheric variables driving the lake models are provided by the nearest onshore stations, and lake data used to validate the model simulations are limited by the poor temporal resolution of the water temperature soundings.

* Corresponding author: marjorie.perroud@unige.ch

Nevertheless, in this study, the underlying hypothesis regarding the application of one-dimensional models will be, to a large extent, verified if at least one model realistically reproduces seasonal temperature profiles when (1) the original model formulation and parameterization do not need to be substantially modified for this particular lake, (2) the driving atmospheric variables do not include any significant ad hoc scaling factors other than the values found in the literature (e.g., the wind multiplication factor; Hornung 2002), and (3) there are no calibration parameters other than those found in the literature.

With this study, we thus aim to evaluate the ability of one-dimensional numerical models, driven by common atmospheric observations, to reproduce thermal characteristics of the deep segment of Lake Geneva in a realistic manner. The choice of the models was undertaken according to three main criteria. The models have to (1) use different approaches to cover a wide range of possible hydrodynamic formulations, parameterizations, and numerical schemes; (2) be widely used; and (3) have shown skill in simulating thermal profiles. The four models tested include one eddy-diffusive lake model, the Hostetler model (hereinafter referred to as HLM); a Lagrangian model, the one-dimensional Dynamic Reservoir Simulation Model "DYRESM"; a k–ε turbulence model, "SIMSTRAT"; and a model based on the concept of self-similarity (assumed shape) of the temperature–depth curve, the Freshwater Lake model "FLake." These models will be described briefly later. Three of them have already been tested on large lakes, yielding satisfactory results (Hostetler and Bartlein 1990; Boyce et al. 1993; Peeters et al. 2002).

In a first phase, calibrations pertaining to each model parameter and adjustments related to the location of the offshore station were carried out on data from three separate years (test samples) before being applied to the 10-yr period under investigation. The comparison assesses monthly temperature profiles averaged over a number of levels in the mixed layer, in the metalimnion, and in the hypolimnion, respectively. It then evaluates the metalimnion's thickness and the strength of the summer stratification.

In this paper is a description of the experimental study site in terms of available lake and atmospheric data, a short description of the model formulations and calibrations, and a definition of the common atmospheric data driving the numerical models, as well the experimental design. Then, a validation of each model on the basis of available high-resolution vertical temperature soundings is presented, and finally, results of the model comparison on the basis of their abilities to simulate the evolution of the monthly thermal characteristics of Lake Geneva are shown.

Methods

Study site—Bordered by the Alps to the south and the Jura mountains to the north, Lake Geneva is located at 46°26′N, 6°33′E (mean geographic position). It is a freshwater body with a surface area of 580 km^2 shared by Switzerland and France, with a maximum length of 73 km and a maximum width of 14 km. It can be divided into two parts: the "Grand Lac" on the eastern side and the "Petit Lac" to the West, in its small and narrow section. The former, with a maximum depth of 309 m, represents more than 96% of the total water volume. Because Lake Geneva remains stratified most of the year and surface waters do not freeze in the main body, it is considered a warm, monomictic lake, although complete winter mixing occurs very rarely in the Grand Lac. The last complete overturns took place consecutively in the winters of 2004–2005 and 2005–2006, 20 yr after the previous overturning (Lazzarotto et al. 2006; Lazzarotto and Rapin 2007). However, the shallower Petit Lac (maximum depth 76 m) mixes every winter.

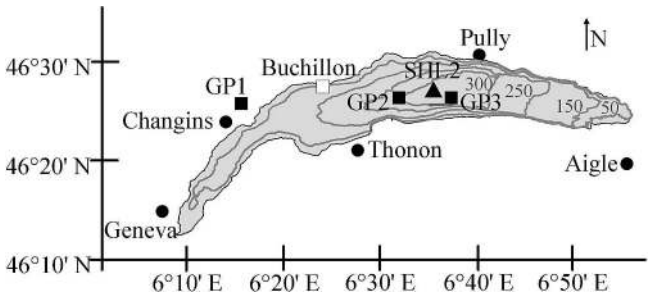

Fig. 1. Map of Lake Geneva (longitude and latitude) with locations of the meteorological stations (black dots) and grid points of the COSMO model (black squares). The position of SHL2 (black triangle) and of a mast 100 m offshore (white squares) are indicated.

The French National Institute for Agricultural Research (INRA) collects bimonthly samples of thermal and biochemical properties of water, such as temperature, conductivity, and oxygen, at a deepest point of the lake (Database INRA of Thonon-Les-Bains, Data CIPEL) within the framework of a monitoring program coordinated by the International Commission for the Protection of Lake Geneva (CIPEL). This station, called SHL2, is located more or less in the middle of the Grand Lac (Fig. 1). Discrete measurements vary slightly within the time period of this study, but are presently recorded at depths of 0, 2.5, 5, 7.5, 10, 15, 20, 25, 30, 35, 50, 100, 150, 200, 250, 275, 290, 300, 305, and 309 m. Additionally, high-resolution vertical temperature soundings ($\Delta z \approx 1$ m) are available for the purpose of this study. They are measured from the surface down to the bottom of the lake by a multiparameter probe ME (Standart-ECO-Probe Version II) up to 2001 and then by a conductivity temperature depth (CTD) 90 multiparameter probe (Sea-Sun Tech).

Penetration of solar radiation in the water column is closely correlated to water transparency. Because no depth-dependent light extinction coefficient, K_e, measurements exist, bimonthly values are deduced on the basis of the Secchi disk depth (Z_{SD}) and interpolated through time to cover the period simulated by the lake models. K_e is then calculated through the Beer–Lambert model with light intensity at depth z corresponding to euphotic depth (1% of surface light intensity). Euphotic depth is estimated to be 2.5 times the Secchi disk depth (Capblancq 1995).

Density stratification of Lake Geneva depends mainly on the vertical water temperature gradients and to a very

minor extent on salinity (here defined with the "practical salinity scale," S), as well as on suspended particles (Umlauf and Lemmin 2005). Even though the effects of these two last are negligible, they have been taken into account in the computation of the water density, ρ_w. In each model, ρ_w depends on water temperature (T_w), S, and depth-induced pressure. Water conductivity, which is proportional to the concentration of dissolved ions, is currently used to derive S. In Lake Geneva, conductivity (normalized at 25°C), κ_{25}, is measured. Composition of seawater and lake water is different; therefore, the practical salinity scale formula (UNESCO 1981; PSS78), which is based on salt water to retrieve salinity from conductivity, cannot be applied. A method has been used that reproduces local density conditions, without changing the density parameterization in each model. The density of Swiss lakes [defined by D. Imboden and R. Kifter (unpubl.) according to lake ionic composition, as per the second term in Eq. 1] has thus been individually equalized with the density equation of each model.

$$\rho_w(T_w, S) = \rho_w(T_w)(1 + \beta_\kappa \kappa_{20}) \quad (1)$$

κ_{20} is then converted into "density-equivalent" salinity by a linear regression of T_w [0–20°C] on S [0–0.5] as per the approach described by Wüest et al. (1996). This approximate freshwater density equation, based on the dominance of ions in Swiss lakes and rivers, namely calcium and bicarbonate, is given through κ_{20} and β_κ, the specific expansion coefficient for κ_{20} through $Ca(HCO_3)_2$. κ_{25} has been changed into κ_{20} by the empiric formula described in Bührer and Ambühl (1975):

$$\kappa_{20} = \kappa_T\left(1.72118 - 0.0541369T + 1.14842 \times 10^{-3} T^2 - 1.222651 \times 10^{-5} T^3\right) \quad (2)$$

with κ_T the conductivity at temperature T.

Model descriptions—Among the range of one-dimensional lake models developed to simulate the evolution of the water temperature profiles, two kinds of models can be distinguished—that is, eddy-diffusion and turbulence-based models. They have all been shown to realistically reproduce multiple aspects of the lake thermal profiles. Therefore, the choice of a specific model depends more on the exact questions to be addressed in the particular study. Eddy-diffusion models simulate the vertical transport of heat in the water with the use of a mixing parameterization based on an eddy-diffusion approach (Orlob and Selna 1970; Henderson-Sellers et al. 1983). Turbulence-based models compute the production and available amount of turbulent kinetic energy, parameterize the vertical transport by eddies (Kraus and Turner 1967; Imberger et al. 1978; Burchard and Baumert 1995), and consider the dissipation of energy.

The models selected for the purpose of this project include an eddy-diffusion model based on a diffusion coefficient, HLM (Hostetler 1987; Hostetler and Bartlein 1990); an updated version of the DYRESM Lagrangian model developed by Imberger et al. (1978); an extended version of the k–ε turbulence model, SIMSTRAT (Goudsmit 2002); and, a bulk model based on two-layer self-similarity, FLake (Mironov 2008). Technical details, calibration, parameter optimization, and other simulation characteristics referring to these models are summarized in Table 1. In addition, governing equations of these models are summarized in Tables 2–5.

Numerical schemes have grown in complexity since earlier one-dimensional lake models considered molecular diffusion of heat the only means of downward transport outside the epilimnion (Dake and Harleman 1969). Parameterizations of vertical mixing have also progressively improved so that the effects of winds on surface layers and of seiching on the meta-hypolimnion are an option for two of these models.

The HLM uses the parameterization of Henderson-Sellers (1985) as an approximation to the eddy-diffusion coefficient. This equation is highly dependent on the surface friction velocity, u_*, obtained from the surface wind speed, v; the aerodynamic drag coefficient, c_D; and the ratio between the strength of the stratification and the shear stress, provided by the depth-dependent Richardson number (Table 2). In this model, heat diffusion is responsible for the evolution of the thermal profiles. Density instabilities are solved by mixing of the unstable layers.

DYRESM is a one-dimensional turbulence model that uses a Lagrangian approach developed by the Centre for Water Research (CWR), University of Western Australia. It is designed to simulate the distribution of heat and salinity in the water column of lakes and reservoirs. The first version has been described in detail by Imberger et al. (1978) and Imberger and Patterson (1981) and has been improved more recently by Yeates and Imberger (2003). The public domain version, DYRESM V4.0.0-b2, is used in this study. DYRESM is structured in layers of uniform properties but of variable thicknesses that need to be defined by the user. Layer mixing occurs when the turbulent kinetic energy (TKE), which is stored in the topmost layers and produced by convective overturn, wind stirring, and shear, exceeds a potential energy threshold (Table 3). Moreover, DYRESM accounts for diffusion created by basin-scale internal waves. It uses the lake number, L_N, to evaluate the amplitude of the internal wave and to parameterize the turbulence created by the damping of the motion of seiches on the bottom boundary and the shear mixing in the interior of the lake.

The third model, SIMSTRAT, the buoyancy-extended k–ε model (Rodi 1984; Burchard et al. 1998), has been updated to include the effects of internal seiches on the production of TKE. Turbulent mixing is solved by the two dependent equations of production and dissipation of TKE (Table 4). The source of TKE is generated by shear stress from the wind and buoyancy production in the case of unstable stratification. Seiching developed under the action of the wind increases TKE in the interior of the lake from a loss of seiche energy by friction at the bottom.

The fourth model, the Freshwater Lake model, or FLake, is based on the concept of the self-similarity of the thermocline structure, drawn from numerous observations of oceanic mixing layer dynamics (Kitaigorodskii and Miropolsky 1970). A two-layer structure is assumed, consisting of a mixing layer with constant temperature

Table 1. Model name, type, calibration, characteristics, and references.*

Model	Type	Calibration and parameter optimization	Simulation characteristics	Other characteristics	Reference
HLM	Energy balance with eddy diffusivity and convective mixing	No calibration $v_{lake} = f(v)$ $C_D = C_{DM} = C_D (v_{lake})$†	Time step = 1 h Archival frequency = 1 d^{-1} Layer depth = 1 m	Inflow and outflow set to 0 Variable K_e	Hostetler and Bartlein 1990
DYRESM	Process-based, vertical mixing as an extension of the Kraus–Turner deepening law (Kraus and Turner 1967)	$v_{lake} = f(v)$ $C_D = 0.0018$ VMC = 700	Time step = 1 h Archival frequency = 1 d^{-1} Layer depth = variable (0.5–3 m)	Lagrangian layer scheme Include seiche parameterization Inflow and outflow set to 0 Constant K_e	Yeates and Imberger 2003 Kraus and Turner 1967
SIMSTRAT	Turbulent kinetic energy production and dissipation Diffusive mixing	$v_{lake} = f(v)$ $C_D = C_D (v_{lake})$ $\alpha_{seiche} = 0.012$ $q = 0.9$	Time step = 10 min Archival frequency = 1 d^{-1} Layer depth ≈ 0.75 m	Include seiche parameterization Inflow and outflow set to 0 Variable K_e	Goudsmit et al. 2002
FLake	Bulk heat and kinetic energy budgets	No calibration Virtual bottom at 60 m if deeper than 60 m $C_D = C_{DM}$†	Time step = 1 h Archival frequency = 1 d^{-1} Layer depth = variable (2 layers: mixing layer and thermocline)	Self-similarity (assumed shape) of the temperature–depth curve No hypolimnion No inflow and outflow Slab model (no bathymetry) Active sediments (optional) Variable K_e	Mironov 2008

* HLM, Hostetler Lake model; v, the hourly wind speed recorded at a land station; v_{lake}, the corresponding wind speed over the lake surface at SHL2.
† Formulation used for momentum drag only.

Table 2. Governing equations of the Hostetler model (Hostetler and Bartlein 1990).

$$\frac{\partial T}{\partial t} = \frac{1}{A(z)}\frac{\partial}{\partial z}\left\{A(z)[\kappa_m + K(z,t)]\frac{\partial T}{\partial z}\right\} + \frac{1}{A(z)}\frac{1}{C_W}\frac{\partial[\Phi A(z)]}{\partial z}$$

$$K(z,t) = \frac{v_k u_* z}{P_0} e^{(-k^* z)}\left(1 + 37\,\mathrm{Ri}^2\right)^{-1}$$

$$u_* = \sqrt{\frac{\rho_a}{\rho_0} c_D v^2}$$

Definitions

$A(z)$	Lake area at depth z (m^2)
c_D	Drag coefficient
C_w	Volumetric heat capacity of water (J m^{-3} °C^{-1})
$K(z, t)$	Eddy diffusivity (m^2 s^{-1})
k^*	Latitudinally dependent parameter of the Ekman profile
P_0	Neutral value of the turbulent Prandtl number (1.0)
t	Time (s)
Ri	Richardson number
T	Water temperature (°C)
v	Wind speed 2 m above the water surface
u_*	Surface friction velocity (m s^{-1})
v_k	von Karman constant (0.4)
z	Depth from the surface (m)
κ_m	Molecular diffusion of water (m^2 s^{-1})
ρ_0	Density of lake surface (kg m^{-3})
ρ_a	Air density (kg m^{-3})
Φ	Heat source term (W m^{-2})

Table 3. Governing processes and equations of the DYRESM model (Yeates and Imberger 2003).

Surface mixed layer

$$\mathrm{KE}_{conv} = \eta_p \rho_j A_{j-1} \omega_*^3 \Delta t$$

$$\mathrm{KE}_{stir} = \eta_s \rho_j A_j u_*^3 \Delta t$$

$$\mathrm{KE}_{shear} = \frac{\eta_k}{2}\frac{M_j M_{j-1}}{M_j + M_{j-1}}\left(U_j - U_{j-1}\right)^2$$

$$u_* = \sqrt{\frac{\rho_a}{\rho_0} c_D v^2}$$

$$\mathrm{PE}_{mix} = g[(M_j + M_{j-1})\zeta_{j-1}^* - (M_j\zeta_j + M_{j-1}\zeta_{j-1})]$$

Deep mixing

$$F_i^T = \frac{200 N_i^2 A_i \kappa_m \Delta t}{L_N N_{max}^2\left(\frac{\delta_i + \delta_{i+1}}{2}\right)}$$

$$F_i^I = \begin{cases} \dfrac{F_i^T \tanh(B_N)(L_N - 1)}{L_N} & L_N > 1 \\ 0 & \text{otherwise} \end{cases} \quad \text{and}$$

$$F_i^B = F_i^T - F_i^I$$

Definitions

A_j	Surface area of layer j (m^2)
A_i	Surface area of layer i below the surface mixed layer (m^2)
B_N	Burger number
C_D	Surface drag coefficient
δ_i	Thickness of layer i below the surface mixed layer (m)
F_i^B	Benthic boundary layer volume exchange (m^3)
F_i^I	Internal volume exchange (m^3)
F_i^T	Total volume exchange between two layers (m^3)
g	Acceleration due to gravity (m s^{-2})
κ_m	Molecular diffusion coefficient for heat (m^2 s^{-1})
KE_{conv}	Turbulent kinetic energy due to convective mixing (kg m^2 s^{-2})
KE_{stir}	Turbulent kinetic energy due to wind stirring (kg m^2 s^{-2})
KE_{shear}	Turbulent kinetic energy due to shear mixing (kg m^2 s^{-2})
L_N	Lake No.
M_j	Mass of layer j (kg)
j	Surface layer index
N^2	Buoyancy frequency squared (s^{-2})
N_{max}^2	Maximum buoyancy frequency squared in a "Portable Flux Profiler" profile (s^{-2})
PE_{mix}	Potential energy to mix layers D and $D-1$ (kg m^2 s^{-2})
U_j	Speed of layer j (m s^{-1})
u_*	Surface friction velocity (m s^{-1})
v_H	Wind speed at height H above the lake surface (m s^{-1})
Δt	Model time step (s)
η_k	Efficiency coefficient associated with the TKE due to shear mixing
η_p	Efficiency coefficient associated with the TKE due to convective mixing
η_s	Efficiency coefficient associated with the TKE due to wind stirring
ρ_a	Air density (kg m^{-3})
ρ_j	Water density at layer j (kg m^{-3})
ρ_0	Density of lake surface (kg m^{-3})
ω^*	Turbulent velocity scale due to convective overturn (m s^{-1})
ζ_j	Center of mass of layer j before mixing (m)
ζ_j^*	Center of mass of layer j after mixing (m)

This model is based on a Lagrangian layer scheme in which the lake is modeled by a series of horizontal layers of uniform property but variable thickness. Mixing is represented by the amalgamation of layers. Properties of the amalgamated layer are volumetrically averaged. When combining two layers, say i and $i + 1$, the conservation laws for a given property, noted C in layer i, such as water temperature, T, salt, S, and momentum, U, can be generalized as

$$C_i^* = \frac{C_i \Delta M_i + C_{i+1}\Delta M_{i+1}}{\Delta M_i + \Delta M_{i+1}}$$

where ΔM is the change of water mass in layer i and $i + 1$. Although this framework remained essentially unchanged, this later version of DYRESM includes a pseudo–two-dimensional benthic boundary layer structure as described above.

and of a thermocline, extending between the mixing layer and the lake bottom. The water temperature shape in the thermocline is parameterized by a fourth-order polynomial function of the depth that depends on a shape coefficient C_T (Table 5). The mixed-layer temperature, the bottom water temperature, the mixed-layer depth, and the shape coefficient C_T determine the water temperature profile. The same concept of parametric shape functions is applied to other elements of lake systems: sediment, ice, and snow

Table 4. Governing equations of the k–ε model and extensions included in SIMSTRAT (Goudsmit et al. 2002).

$$\frac{\partial T}{\partial t}=\frac{1}{A}\frac{\partial}{\partial z}\left[A(v_t'+\kappa_m)\frac{\partial T}{\partial z}\right]+\frac{1}{\rho_r c_p}\frac{\partial H_{sol}}{\partial z}+\frac{\partial A}{\partial z}\frac{H_{geo}}{A\rho_r c_p}$$

$$\frac{\partial U_u}{\partial t}=\frac{1}{A}\frac{\partial}{\partial z}\left[A(v_t+v)\frac{\partial U_u}{\partial z}\right]+fU_v$$

$$\frac{\partial U_v}{\partial t}=\frac{1}{A}\frac{\partial}{\partial z}\left[A(v_t+v)\frac{\partial U_v}{\partial z}\right]-fU_u$$

$$\frac{\partial k}{\partial t}=\frac{1}{A}\frac{\partial}{\partial z}\left(Av_k\frac{\partial k}{\partial z}\right)+P+P_{seiche}+B-\varepsilon$$

$$\frac{\partial \varepsilon}{\partial t}=\frac{1}{A}\frac{\partial}{\partial z}\left(Av_\varepsilon\frac{\partial \varepsilon}{\partial z}\right)+\frac{\varepsilon}{k}[c_{\varepsilon 1}(P+P_{seiche})+c_{\varepsilon 3}B-c_{\varepsilon 2}\varepsilon]$$

$$P=v_t\left[\left(\frac{\partial U_u}{\partial z}\right)^2+\left(\frac{\partial U_v}{\partial z}\right)^2\right]\qquad B=-v_t'N^2$$

$$v_t=c_\mu\frac{k^2}{\varepsilon}\qquad v_t'=c_\mu'\frac{k^2}{\varepsilon}$$

$$v_k=\frac{c_\mu}{\sigma_k}\frac{k^2}{\varepsilon}\qquad v_\varepsilon=\frac{c_\mu}{\sigma_\varepsilon}\frac{k^2}{\varepsilon}$$

$$\tau=\frac{c_D\rho_a}{\rho_0}v_u^2+v_v^2$$

	Definitions		Constant of the k–ε model
A	Cross-sectional area at z (m^2)		
B	Buoyancy flux (W kg^{-1})	$c_{\varepsilon 1}$	1.44
c_p	Specific heat of lake water (J kg^{-1} K^{-1})	$c_{\varepsilon 2}$	1.92
c_D	Surface drag coefficient		
f	Coriolis parameter (s^{-1})	$c_{\varepsilon 3}$	-0.4 if $B<0$, else 1
t	Time (s)		
k	Turbulent kinetic energy per unit of mass (J kg^{-1})	c_μ	0.09
H_{sol}	Solar radiation at depth z (W m^{-2})	c_μ'	0.072
H_{geo}	Geothermal heat flux (W m^{-2})	σ_k	1.00
N	Brunt–Väisälä frequency (s^{-1})	σ_ε	1.3
T	Water temperature (°C)		
v_u	Horizontal air velocity west–east (m s^{-1})		
U_u	Horizontal velocity west–east (m s^{-1})		
v_v	Horizontal air velocity south–north (m s^{-1})		
U_v	Horizontal velocity south–north (m s^{-1})		
P	Production of k due to shear stress (W kg^{-1})		
P_{seiche}	Production of k due to internal seiche (W kg^{-1})		
z	Depth (positive upward, m)		
ε	Dissipation rate of k (W kg^{-1})		
ρ_a	Air density (kg m^{-3})		
ρ_r	Reference density of lake water (kg m^{-3})		

Table 4. Continued.

	Definitions	Constant of the k–ε model
ρ_0	Density of lake surface (kg m^{-3})	
τ	Surface wind stress (m^2 s^{-2})	
v	Molecular viscosity, 1.5×10^{-6} m^2 s^{-1}	
κ_m	Molecular diffusivity, 1.5×10^{-7} m^2 s^{-1}	
v_t	Turbulent viscosity (m^2 s^{-1})	
v_t'	Turbulent diffusivity (m^2 s^{-1})	
v_ε	Turbulent diffusivity of ε (m^2 s^{-1})	
v_k	Turbulent diffusivity of k (m^2 s^{-1})	

layers, with linear shape functions for ice and snow. The model calculates the temporal evolution of an ensemble of lake structure parameters that balance thermal fluxes on internal and external boundaries. The mixed-layer depth dynamics include convective entrainment, wind-driven mixing, and volumetric solar radiation absorption. The two-layer water thermal structure used in FLake precludes its application to deep lakes because the hypolimnion is usually present between the thermocline and the lake bottom. To avoid this limiting factor, a virtual

Table 5. Governing equations of FLake model (Mironov 2008). The shape of the water temperature profile is prescribed; the self-consistent profiles, described by the universal nondimensional functions Φ, are used.

$$T(z)=\begin{cases}T_{surf} & 0\le z\le h\\ T_{surf}-(T_{surf}-T_{bot})\Phi_T(\zeta) & h\le z\le D\end{cases}$$

$$\Phi_T(\zeta)=\left(\frac{40}{3}C_T-\frac{20}{3}\right)\zeta+(18-30C_T)\zeta^2+(20C_T-12)\zeta^3+\left(\frac{5}{3}-\frac{10}{3}C_T\right)\zeta^4$$

$$\zeta=\frac{z-h}{D-h}$$

$$u_*=\sqrt{\frac{\rho_a}{\rho_0}c_D v^2}$$

	Definitions	Other characteristics
c_D	Drag coefficient	
C_T	Shape parameter	
h	Mixed-layer depth (m)	
T	Water temperature (°C)	D = virtual bottom at 60 m
T_{surf}	Surface water temperature (°C)	
T_{bot}	Bottom water temperature (°C)	
v	Wind speed 2 m above the water surface	
z	Depth (m)	
u_*	Surface friction velocity (m s^{-1})	
ρ_a	Air density (kg m^{-3})	
ρ_0	Density of lake surface (kg m^{-3})	

Table 6. Hourly meteorological value recorded at Changins over the 10-yr period 1996–2005.

	T (°C)	v (m s^{-1})	H_r (%)	$QS\downarrow$ (W m^{-2})	p (hPa)
Mean	10.6	2.3	73.2	142	966
Minimum	−10.7	0	13.4	0	928
Maximum	36.3	17.8	100	1040	988

H_r, relative humidity; $QS\downarrow$, incident solar radiation; p surface pressure.

bottom is usually placed at 60 m whenever lake depth exceeds 60 m.

Meteorological data—Lake models need to take into account components of the energy budget, as well as other atmospheric variables and their evolution in time. The energy transfer that drives these models is based on the surface energy budget, computed as $QS^* + QL^* - (Q_E + Q_H)$, and on the wind stress forcing. The energy budget involves net solar radiation, $QS^* = QS\downarrow - QS\uparrow$, taking into account incoming solar radiation, $QS\downarrow$, and reflected solar radiation, $QS\uparrow$; the net atmospheric infrared radiation, $QL^* = QL\downarrow - QL\uparrow$, considering the infrared radiation emitted by the atmosphere down to the surface, $QL\downarrow$, and the infrared flux released by the surface, $QL\uparrow$; and, finally, the latent (Q_E) and sensible heat (Q_H) fluxes. Positive values of the latter indicate heat extraction from the lake to the atmosphere. These components are computed as common inputs to the lake models, but incident solar radiation, $QS\downarrow$, is prescribed from observations.

The required meteorological variables are provided as hourly values of air temperature, T, horizontal wind magnitude, v, relative humidity, H_r, and cloud cover, C. Meteorological records in the vicinity of the lake are supplied by the Automatic Network (ANETZ) of the Federal Office of Meteorology and Climatology, MeteoSwiss (Bantle 1989), and by a MeteoFrance inland weather station nearby. Locations of the four land stations are indicated in Fig. 1. Meteorological inputs used to drive the models are taken from the land station Changins because of its central location and because its wind data are not perturbed by surrounding land surface characteristics (Table 6). Surface air temperatures were adjusted according to the station altitude differences compared with the water surface of the lake. To remove the bias of inland wind speed recordings and to generate values over open water at station SHL2, a correction factor has been implemented. It takes into account wind outputs from a numerical weather forecast model, COSMO (Consortium for Small-scale Modeling; Bettems 2002) provided by MeteoSwiss at three model grid points (GP1, GP2, and GP3, respectively, as shown in Fig. 1).

A common parameterization based on the bulk transfer method has been employed for the surface sensible and latent heat fluxes. The scheme uses the atmospheric vapor pressure, e_a (hPa), computed on the basis of H_r (%) and on the saturation vapor pressure e_0 (hPa) function of the surface air temperature. Hostetler and Bartlein (1990) propose to use Richards' equation (1971) to compute e_0, as follows:

$$e_0 = 1013.25e^{\left(13.3185t_K - 1.976t_K^2 - 0.6445t_K^3 - 0.1299t_K^4\right)} \quad (3)$$

where

$$t_K = 1 - \left[\frac{373.15}{T_w + 273}\right] \quad (4)$$

Infrared radiation flux density emitted by the water surface is approximated by the Stefan Boltzmann law with water emissivity set to 0.97 in all models (Henderson-Sellers 1986). Downward atmospheric infrared radiation to the water surface is given by standard formulation based on ε_a, effective atmospheric emissivity. A wide range of formulations to calculate ε_a have been compared and presented in detail in Henderson-Sellers (1986). The formulation for ε_a that depends on the cloud cover fraction, C, is proposed by Hostetler and Bartlein (1990) as follows:

$$\begin{aligned}\varepsilon_a &= 0.84 - \left(0.1 - 9.973\times10^{-6}e_a\right)(1-C)\\ &\quad + 3.491\times10^{-5}e_a \qquad 1-C \geq 0.4\end{aligned} \quad (5a)$$

$$\begin{aligned}\varepsilon_a &= 0.87 - \left(0.175 - 29.93\times10^{-6}e_a\right)(1-C)\\ &\quad + 2.693\times10^{-5}e_a \qquad 1-C < 0.4\end{aligned} \quad (5b)$$

The cloud cover fraction is taken as the mean value between two station observations, Geneva and Aigle, that is located east of the lake.

The albedo, α, that is used to compute the solar flux reflected at the surface accounts for the solar zenith angle and the solar declination angle (Bonan 1996),

$$\alpha = 0.05(\mu + 0.15)^{-1} \quad (6)$$

with μ as the cosine of the local solar zenith angle.

Experimental setup

The four models are run in a standalone mode over lake Sta. SHL2, wherein a common set of atmospheric driving variables are prescribed for a 10-yr period on an hourly basis. To compare simulated lake profiles, observed or derived values of T, $QS\downarrow$, $QL\downarrow$, v, and e_a for the period 1996–2005 are used as input variables for the models, also on an hourly basis. A common module then explicitly computes $QS\uparrow$, $QL\uparrow$, Q_E, and Q_H at each time step. The transfer of energy from wind to water has been standardized by using the friction velocity, u_*, defined in Tables 2–5. The only difference regarding input variables concerns the light extinction coefficient. The user's interface of DYRESM does not allow modifying the value, which is set to the annual average. The morphometry is common to all models and consists of height–area values characteristic of the waterbody, as illustrated in Fig. 1.

Because of the low frequency of complete turnover in Lake Geneva, an initial homogenized temperature and salinity profile cannot be used because it would create shifts that cannot easily be recovered during the following seasons. The previously described vertical profiles of water

temperature and salinity conducted at SHL2 were used to initialize the conditions prevailing in the lake at the beginning of simulations. Each yearly simulation runs from the last sounding of the previous year to 31 December of the following year. Each model has its own time-marching scheme and time step interval. Water temperature profiles were archived daily at the exact same time to facilitate comparison.

Model calibrations and wind speed adjustment—The calibration phase initially focuses on specific model parameters that cannot be inferred from measurements (Table 1). Because buoys do not record meteorological variables at the center of the lake, it remains difficult to assess the specific influence that each driving variable produces. Therefore, no calibration procedure is undertaken on those components because the error is detrimental to all models. However, because surface roughness could be considerably different over land than it is over water, a correction to the hourly wind speed values is allowed. Additionally, a drag coefficient is adjusted because of large uncertainties in the roughness height over the water surface.

The calibration considers a sample of three disconnected years: 1996, 2000, and 2004. For calibration, simulated data ($\mathrm{Tsim_w}$) are compared to bimonthly observed temperature profile ($\mathrm{Tobs_w}$) over m layers (l). Validation and model comparison are made on the basis of observed and simulated water temperatures, in which the root mean square of the errors (T_{rmse}), the mean error (T_{me}), the standard variation of the error (T_{stdev}), and the improvement of the T_{rmse} by calibration, $\mathrm{Imp_{rmse}}$ (%) are computed as follows:

$$\mathrm{error}(t_i, l_j) = \mathrm{Tsim_w}(t_i, l_j) - \mathrm{Tobs_w}(t_i, l_j) \tag{7}$$

$$T_{\mathrm{me}} = \frac{1}{\sum_{i=1}^{n} m_i} \sum_{i=1}^{n} \sum_{j=1}^{m_i} \left[\mathrm{error}(t_i, l_j)\right] \tag{8}$$

$$T_{\mathrm{stdev}} = \sqrt{\left\{ \frac{1}{\sum_{i=1}^{n} m_i - 1} \sum_{i=1}^{n} \sum_{j=1}^{m_i} \left[\mathrm{error}(t_i, l_j) - T_{\mathrm{me}}\right]^2 \right\}} \tag{9}$$

$$T_{\mathrm{rmse}} = \sqrt{\left[\frac{1}{\sum_{i=1}^{n} m_i} \sum_{i=1}^{n} \sum_{j=1}^{m_i} \mathrm{error}(t_i, l_j)^2 \right]} \tag{10}$$

$$\mathrm{Imp_{rmse}} = 100 - \left[\left(\frac{T_{\mathrm{rmse\_cal}}}{T_{\mathrm{rmse\_ref}}} \right) 100 \right] \tag{11}$$

where $j = 1, 2, \ldots, m$; $i = 1, 2, \ldots, n$; n is the number of days in which a sounding has been taken, and $T_{\mathrm{rmse\_ref}}$ and $T_{\mathrm{rmse\_cal}}$ are the T_{rmse} before and after calibration.

To characterize the thermal layers with some degree of accuracy, the water column was partitioned into three groups of depths: GD1 (0–10 m), GD2 (15–35 m), and GD3 (50–300 m). Model calibrations were performed through the optimization of values. The optimal value of all specific parameters is determined through minimizing the three annual T_{rmse} compared with a reference value (i.e., before calibration).

The large surface area of Lake Geneva and the topography of its surroundings cause wind speed and direction to be spatially heterogeneous with regard to the scale of the processes that initiate them (Lemmin and D'Adamo 1996). A correction factor to observed values is determined to remove the bias in the wind speed generated by the inland station as a surrogate to SHL2 winds. Hourly data simulated by the COSMO model for 2004 serves to establish this factor. Two linear regressions that use wind speeds at the closest land grid to Changins (GP1) and on those at grid points near SHL2, GP2, and GP3 are determined. The resulting average regression gives a linear relation for wind forcing v of the form for SHL2,

$$v = 0.47 + 1.04 v_{\mathrm{land}} \tag{12}$$

where v_{land} is the wind speed recorded inland at Changins.

The varying wave height that is a function of the aerodynamic drag coefficient, c_{D}, is optimized (Table 1). Momentum exchange from wind to water is parameterized by default with the use of a constant drag coefficient. As reported in Wüest and Lorke (2003), typical values of c_{D} as a function of wind speed vary from 0.0011 for 5 m $\mathrm{s^{-1}}$ to 0.0021 for 25 m $\mathrm{s^{-1}}$—the latter for well-developed waves. Nevertheless, the state of wave saturation is generally never reached in lakes in which wind stress on the surface is limited and with short fetch. Studies have demonstrated that surface roughness increases when young waves are growing (Geernaert et al. 1987; Smith et al. 1992). Thus, c_{D} can largely exceed values for open waters with a long fetch. In Lake Geneva, Graf et al. (1984) have analyzed drag with respect to wave heights at a mast located 100 m offshore of station Buchillon (Fig. 1), a data set for wind speed ranging from 7 to 17.5 m $\mathrm{s^{-1}}$. Consequently, c_{D} is greater over Lake Geneva than the reference value. Thus, at 17.5 m $\mathrm{s^{-1}}$, c_{D} is 0.0027. For wind speeds below 3 m $\mathrm{s^{-1}}$, Bradley et al. (1991) and Lin et al. (2002) have shown that c_{D} increases unexpectedly with decreasing wind speeds. To consider the key role of c_{D} in momentum transfer to the water and its implications for the process of mixing, a nonconstant value for c_{D} has been used to consider the increased values at extremes of both high and low wind speed. Simulations included an empirical drag parameterization for low wind speeds (from 3 m $\mathrm{s^{-1}}$, c_{D} increases as wind speed decreases; Wüest and Lorke 2003) and an extra one obtained during the Lake Geneva campaign for higher wind speeds (Graf et al. 1984) and that correlates c_{D} with the increase of wind speed.

In HLM, changes in the value of the momentum drag coefficient c_{D} can be undertaken only through the parameterization of surface friction velocity. However this procedure does not modify the T_{rmse} to any significant extent. Temperature profiles are slightly improved by

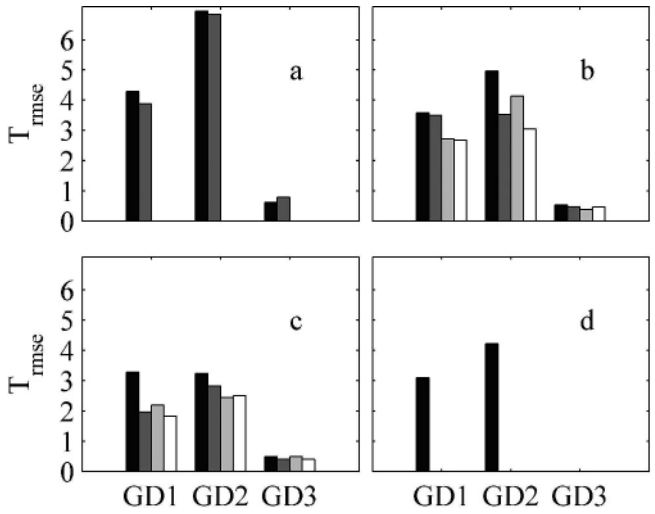

Fig. 2. Mean of T_{rmse} (1996), T_{rmse} (2000), and T_{rmse} (2004) for GD1 (first group of bars), GD2 (second group of bars), and GD3 (third group of bars) according to (a) HLM, in black: no calibration, v_{land}; in dark gray: v; (b) DYRESM, in black: no calibration, VMC = 200, $c_D = 0.0013$, v_{land}; in dark gray: VMC = 500, $c_D = 0.0022$, v_{land}; in light gray: VMC = 200, $c_D = 0.0013$, v; in white: VMC = 700, $c_D = 0.0018$, v; (c) SIMSTRAT, in black: no calibration, $\alpha_{seiche} = 0.006$, $c_D = 0.0013$, $q = 0.75$, v_{land}; in dark gray: $\alpha_{seiche} = 0.013$, c_D taken from Graf et al. (1984) and Wüest and Lorke (2003), $q = 0.9$, v_{land}; in light gray: $\alpha_{seiche} = 0.006$, $c_D = 0.0013$, $q = 0.75$, v; in white: $\alpha_{seiche} = 0.012$, c_D taken from Wüest and Lorke (2003), $q = 0.9$, v; and (d) FLake, in dark gray: no calibration, v_{land}.

scaling the wind speed according to Eq. 12 in GD1 and GD2 (for both, improvement of 4%; Fig. 2a).

DYRESM is considered as a calibration-free model, containing generic parameters that are obtained by field measurement or lab experiments (Hornung 2002; Gal et al. 2003; Hamilton and Schladow 1997). However, it is possible to calibrate the vertical mixing coefficient (VMC) used in the formulation of vertical heat diffusion, in addition to layer thickness defined by the user (Hornung 2002; Yeates and Imberger 2003; Tanentzap et al. 2007). Although generic values normally do not need any modification, parameters related to formulations of TKE in the surface mixed layer (Table 3, e.g., shear production efficiency) have also been varied with the values found in the literature (Gal et al. 2003; Yeates and Imberger 2003; Tanentzap et al. 2007). The VMC is set to 200 by default, a value found empirically by Yeates and Imberger (2003). Simulations were performed with VMC varying from 200 to 1500. In addition, the maximum layer thickness was set from 1 to 5 m. With a minimum layer thickness set to 0.5 m (Hornung 2002), the smallest T_{rmse} were found for maximum thicknesses of 3 m and of 3.5 m (not shown). Then, a range of values for VMC and c_D (because wind-dependent c_D cannot be implemented in this version of the model) are tested with and without the wind correction factor. Increasing c_D and VMC decreases slightly the T_{rmse} in GD1 (improvement of 2%) and reduces it further in GD2 (improvement of 28%; Fig. 2b). When the wind correction factor is added, the T_{rmse} decrease significantly (25% in GD1 and 48% in GD2). These results emphasize the lack of heat penetration before calibration and the need to increase the intensity of the mixing process. In GD3, small values of T_{rmse} are also affected by varying these three parameter values (improvement of 12% without wind correction and 33% with wind correction). Improvements of T_{rmse} in GD1 and GD2 are found with a doubling of the shear production efficiency (0.8) and of the wind stirring (0.12). However, they remain very low, below 5% and 10%, respectively, and do not concern each of the calibrated years. Consequently, modifications in the parameter files are not justified. The sensitivity of the model to variations of the constant light extinction coefficient was tested to assess whether the constant imposed by DYRESM might affect the quality of the results. DYRESM was run with various values of K_e distributed around the annual average value ($\pm 50\%$). Whereas a strong decrease of K_e tends to reduce the error in GD1 and GD2, simulations with higher K_e do not improve the thermal profile. The maximum improvement (7% in GD1 and 21% in GD2) represents a 50% decrease of K_e but is not representative of real conditions, in that this is what is observed during the period of minimum turbidity and would imply no biological effects on light penetration. For a more realistic decrease of K_e (25%) in GD1 and GD2, there is a gain of about 1%, but predicted temperatures are clearly less accurate in GD3.

SIMSTRAT uses two parameters related to the seiche activity, α_{seiche} and q. The former determines the fraction of energy transferred by the wind to the seiche motion and the latter determines the vertical distribution of energy loss from the seiching motion (Goudsmit et al. 2002). The two c_D parameterizations, described above, for both high and low wind speeds are implemented in the model code and tested both separately and jointly. Whether or not a correction to wind speeds is applied, T_{rmse} are reduced at all depths with stronger α_{seiche} (Fig. 2c). With the use of wind observations at the Changins station, the error is further reduced when both c_D parameterizations are included (improvement of 52% in GD1, 35% in GD2, and 8% in GD3). However, when Eq. 12 is used, even smaller T_{rmse} are found when only the low–wind speed parameterization is employed for c_D (improvement of 56% in GD1, 41% in GD2, and 9% in GD3). In fact, when the c_D parameterization for high wind speed minimizes the T_{rmse} in GD2, the latter increases in GD1. Because slight shifts of the thermocline produce high T_{rmse}, it was decided to favor the c_D parameterization for low wind speed. Higher wind speeds compensate for the decrease of energy induced by lower values of c_D (Fig. 2c).

The FLake model does not require any particular calibration. The water surface roughness length is calculated with respect to wind velocity according to the Charnock (1955) formula, wherein the Charnock parameter is obtained from the wind fetch with the use of an empirical equation. The wind fetch used as the model input parameter is no longer required because a common formulation for the momentum flux has been introduced into the models, and c_D becomes a parameter that can be adjusted if required. The high T_{rmse} in GD1 and particularly in GD2 (Fig. 2d) means

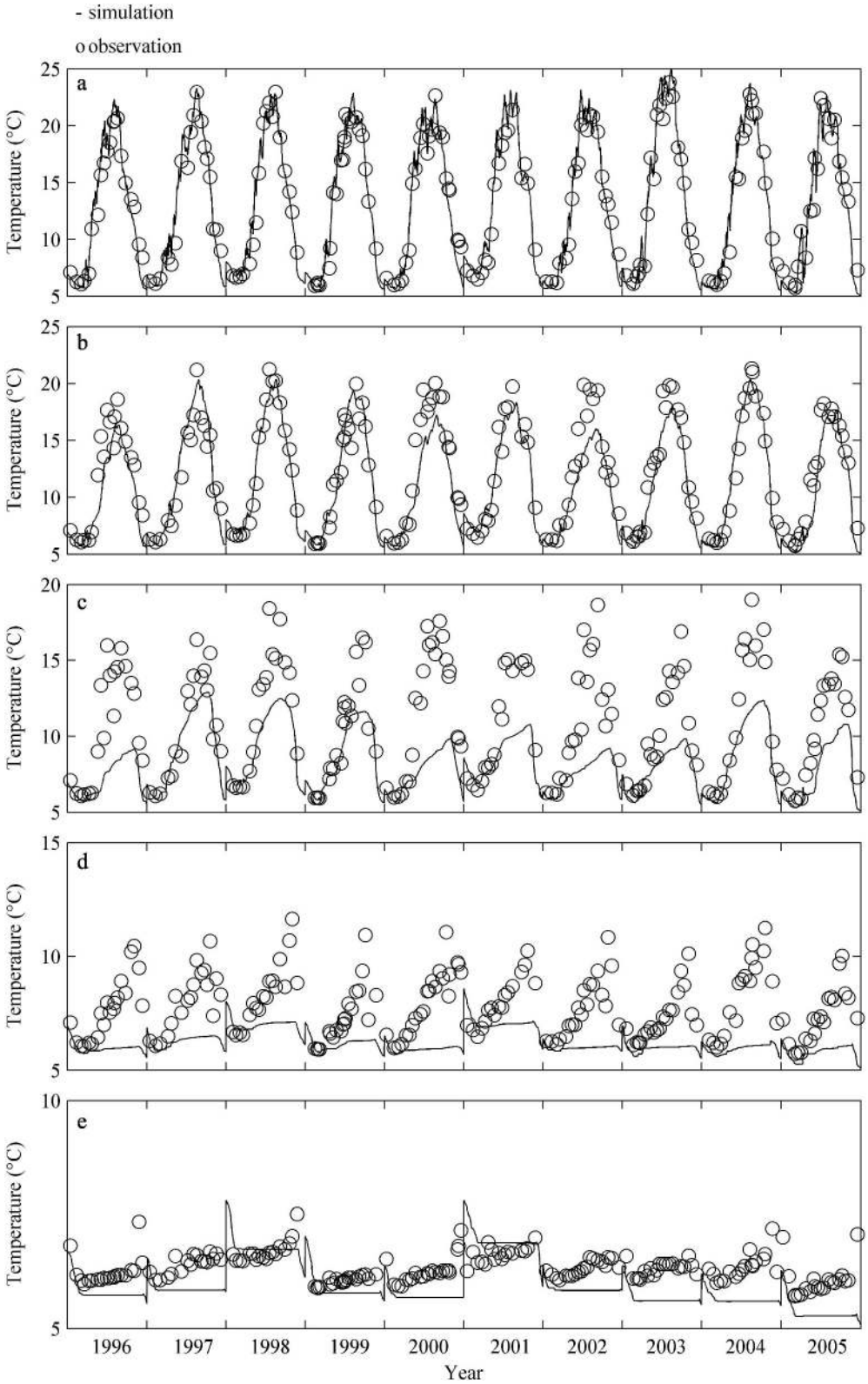

Fig. 3. HLM-simulated water temperatures and observed temperatures averaged over the intervals (a) 0–5 m, (b) 5–10 m, (c) 10–15 m, (d) 15–50 m, and (e) 50–100 m from 01 January 1996 to 31 December 2005.

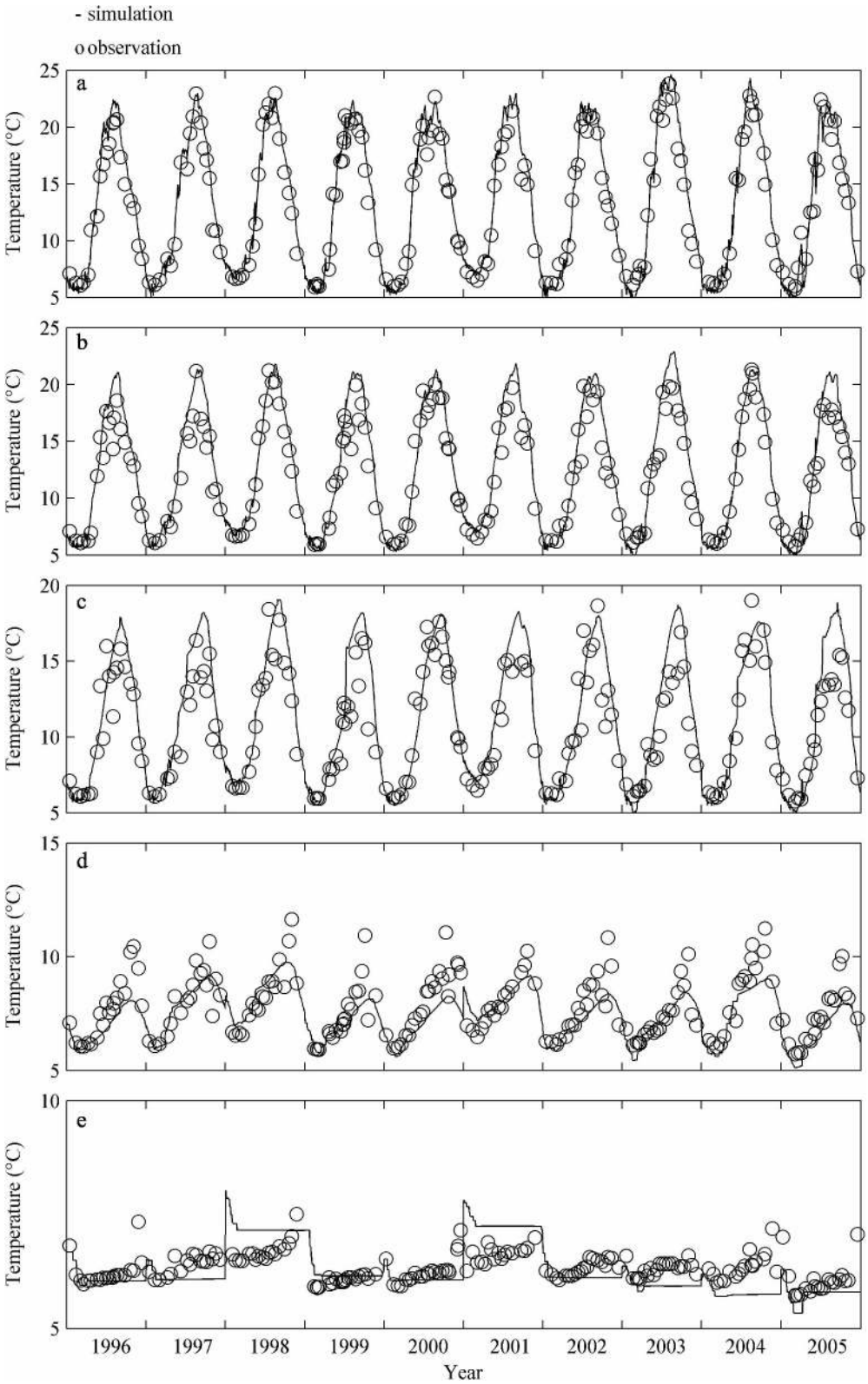

Fig. 4. As in Fig. 3, except for the DYRESM model.

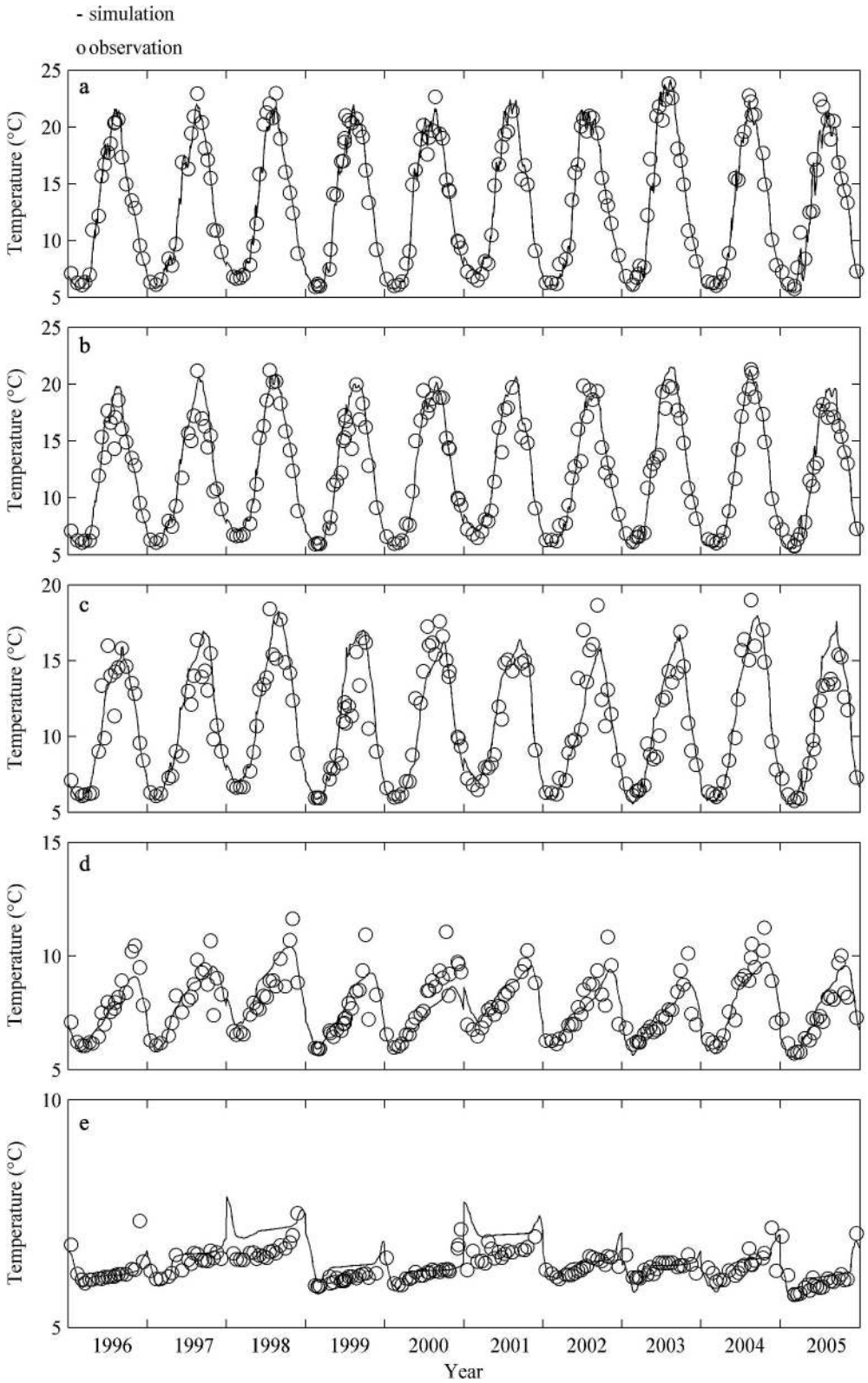

Fig. 5. As in Fig. 3, except for the SIMSTRAT model.

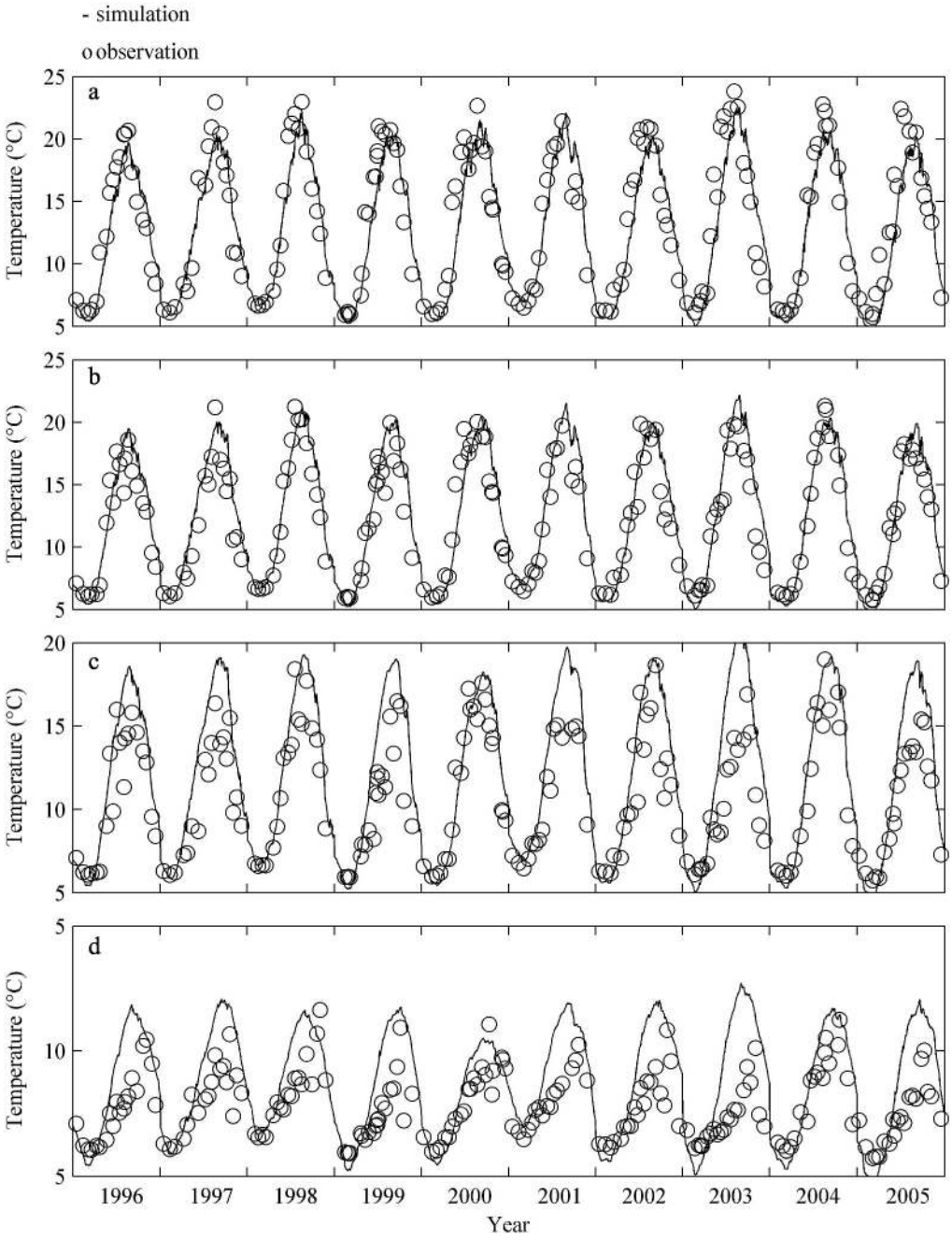

Fig. 6. As in Fig. 3, except for the FLake model and without depth interval e.

that too much heat penetrates deeper layers and implies that further mixing is not necessary.

Validation—The model comparison was carried out on a bimonthly basis of high-resolution vertical soundings over a 10-yr period from 1996 to 2005. Temperature profiles were reset at the beginning of each annual run with the last lake sounding of the previous year. Hence, a bias in the thermal profile produced one year does not affect the following year's simulation. The optimal parameter values were prescribed after minimizing T_{rmse} in the calibration procedure. Simulated temperature profiles were analyzed in terms of time and depth averages (Figs. 3–6). The five depth classes are 1–5 m (D_{0-5}), 5–10 m (D_{5-10}), 10–15 m (D_{10-15}), 15–50 m (D_{15-50}), and 50–100 m (D_{50-100}). Depths below 100 m were not taken into account in the validation because water temperatures did not vary significantly over an annual cycle. Surface temperature is also an important variable that requires validation. The strength and the onset of stratification are thermodynamic aspects of the lake that were considered in the model validation with respect to their essential role in biological processes, particularly for studying species composition, abundance, and distribu-

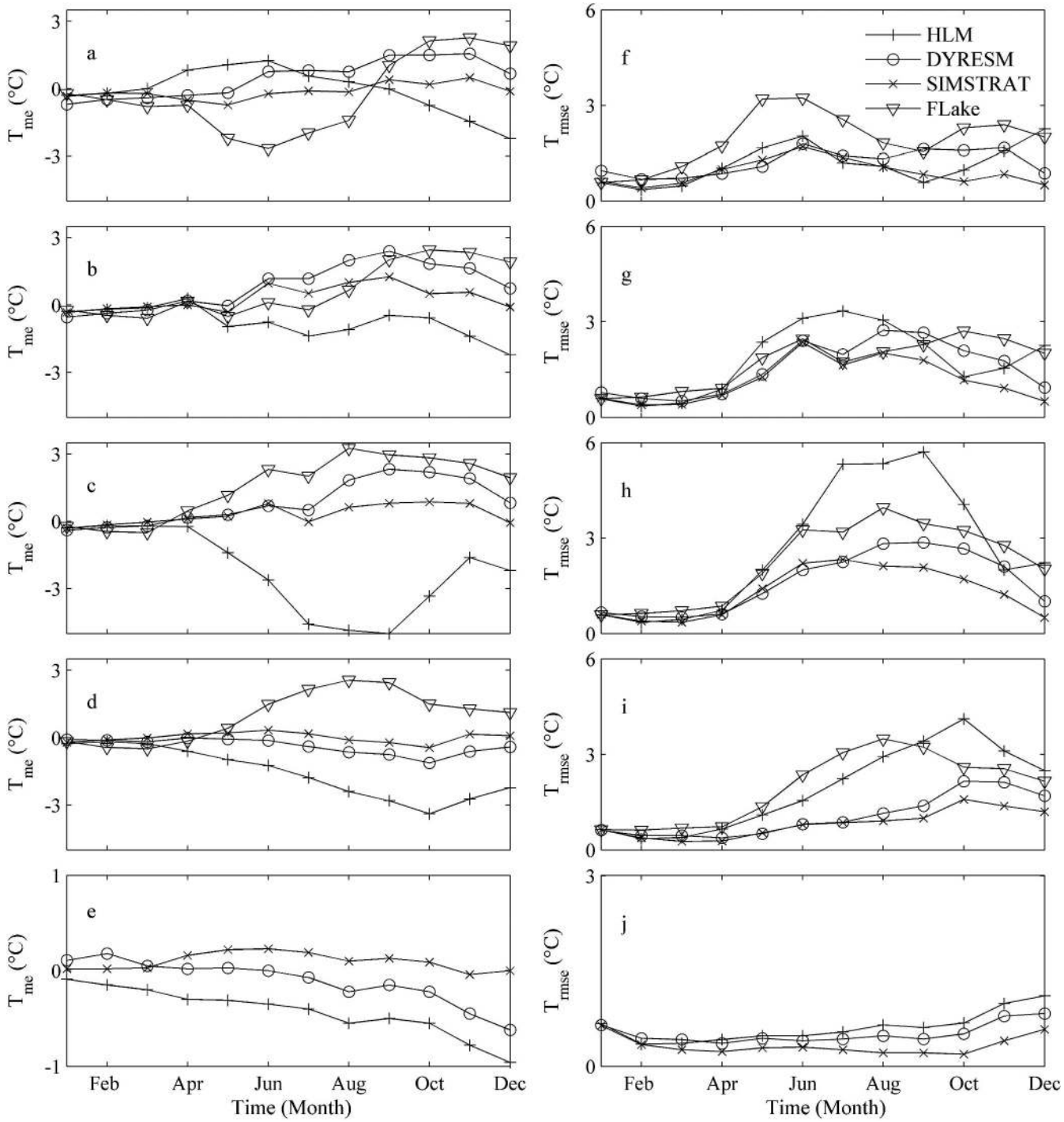

Fig. 7. Monthly mean HLM, DYRESM, SIMSTRAT, and FLake T_{me} (first row) and T_{rmse} (second row) for depth intervals (a, f) 0–5 m, (b, g) 5–10 m, (c, h) 10–15 m, (d, i) 15–50 m, and (e, j) 50–100 m from 01 January 1996 to 31 December 2005.

tion. In addition, these characteristics are associated with the thickness of the metalimnion and serve to explain the temperature errors that arise in the simulated profiles. The stability of the water column with respect to small vertical displacements was deduced from the Brunt–Väisälä frequency N (s^{-1}) as

$$N^2 = \frac{g}{\rho_w}\left(\frac{d\rho_w}{dz}\right) \tag{13}$$

in which g is the acceleration due to gravity and z the depth, and ρ_w was calculated from the UNESCO (1981) equation

of state function of T_w, S, and hydrostatic pressure. Here S is fixed at 0.

A diagnostic index for the onset of thermal stratification (Jacquet et al. 2005) has been reformulated for Lake Geneva. The maximum depth at which a 1°C difference appears between the 100- and 2-m layer is used to diagnose the lowest bound of the metalimnion, M_{LB}, as well as the first occurrence of M_{LB}, to date the beginning of stratification for each simulated year.

Results

As stated previously, the different adjustable parameters and model configurations make a simple comparison difficult. Because of the different parameter values and parameterization schemes used for VMC, α_{seiche}, q, and c_D we will focus on the ability of the models to reproduce the monthly mean temperature profiles, the strength of stratification, and M_{LB} over a 10-yr period. The T_{rmse} and T_{me} were used to evaluate the water temperature differences between observed and simulated data (Fig. 7).

In Fig. 3 and those that follow, the observed water temperature soundings show strong seasonal variations at Sta. SHL2 and are characterized by a seasonal lag and reduced amplitude with increasing depth. From $D_{0–5}$ to $D_{50–100}$, the lowest mean temperatures were recorded in February–March, lying between 6.0°C and 6.5°C. The warmest mean temperatures, 21.3°C and 18.9°C for the depth classes $D_{0–5}$ and $D_{5–10}$, respectively, were recorded in August. In deep layers, the observed delay in the seasonal occurrence of maximum temperatures is caused by the finite heat diffusion and thus generates the warmest temperatures in September in $D_{10–15}$ at 15.6°C and in October in $D_{15–50}$ at 9.7°C. Below 50 m, seasonal variation is less pronounced, with a mean change of only +0.6°C in November. In summer, when the thermocline is well established, ΔT_w between $D_{0–5}$ and $D_{50–100}$ is roughly 15°C, and the strength of stratification, N^2, reaches 2.7×10^{-3} s^{-2}. Onset of stratification, with the first occurrence of M_{LB}, usually takes place between 20 March and 20 April, on average; this interval is based on the observed bimonthly high-resolution temperature profiles.

HLM—The HLM performs well in $D_{0–5}$ (Fig. 3a) with monthly T_{rmse} generally below 1°C, except during the months of May–June and November–December, in which higher values (1.5–2°C) coincide with the stratification and destratification periods. This model's annual mean bias ± SD is 0.08°C ± 1.25°C. In $D_{5–10}$, T_{rmse} exceeds 2°C from May to September, with a maximum of 3.4°C in July, and in $D_{10–15}$ from May to December, with a maximum of 5.7°C in September. These T_{rmse} correspond to monthly T_{me}, respectively, of −0.5°C ± 2.3°C to −1.38°C ± 3.05°C and of −1.40°C ± 1.42°C to −5.00°C ± 2.77°C, thus indicating systematic underestimation of the simulated temperatures over this 10-yr period (Fig. 3b,c). This underestimation is the result of an HLM-simulated metalimnion that is thinner than observed. In Fig. 8a, it is noticed that M_{LB} values stand close to 20 m during the whole period of stratification, whereas observations show that those limits should deepen down to 50 m. Therefore, this model overestimates the maxima of N^2 (Fig. 9a), reducing the heat diffusion in deeper layers (Fig. 3d). Any deep-water variations are then generated only by winter turnover (Fig. 3e).

DYRESM—DYRESM effectively simulates surface layer water temperatures (Fig. 4a) and produces small monthly T_{rmse}, from 0.5°C to 1.7°C, in $D_{0–5}$, wherein monthly T_{me} is positive. Annual T_{me} during these 10 yr is 0.5°C ± 1.2°C. During the warm season, the values of T_{rmse} increase at all depths and reach close to 3°C in $D_{5–10}$ and $D_{10–15}$; this bias is due to overestimations of temperature (Fig. 4b,c), with maxima of T_{me} in August of 2.00°C ± 1.88°C and 1.84°C ± 2.15°C, respectively. On the contrary, in $D_{15–50}$, the maximum T_{rmse} in October over 2°C, jointly with a T_{me} of −1.12°C ± 1.84°C, indicates that the model underestimates the temperatures; in this case, the difference could be due to insufficient heat diffusion from above (Fig. 4b–d), as explained by the positive surface temperature bias. Even though increased mixing during model calibration tends to reduce T_{rmse} in the lower metalimnion (GD2), there is not sufficient heat diffusion in the deeper layers after the onset of stratification. Simulated and observed M_{LB} correlate in spring (Fig. 8b). Later in the season, the M_{LB} shows that the deepening rate of the thermocline is too low, even though the values of N^2 are simulated realistically (Fig. 9b). Below 50 m, where observations indicate a slight increase of water temperature, simulated values do not exhibit any significant variation, with the exception of a temperature adjustment that produces a rapid cooling following the yearly initialization (Fig. 4e).

SIMSTRAT—In $D_{0–5}$, T_{rmse} between 0.5°C and 1.3°C indicate that temperatures are realistically simulated (Fig. 5a). Small monthly T_{me} indicate that no systematic bias exists, corresponding to an annual T_{me} of −0.12°C ± 1.02°C. As is the case with DYRESM, the same behavior with depth is simulated (Fig. 5b–d), producing highest T_{rmse} during the warm season but of smaller magnitude (Fig. 7g,h). Thus, T_{rmse} lie closer to 2°C in $D_{5–10}$ and in $D_{10–15}$. The maximum of T_{rmse} is also reached in October at 1.5°C in $D_{15–50}$. In terms of T_{me}, maxima are, respectively, 0.97°C ± 2.15°C in $D_{5–10}$, 0.80°C ± 2.07°C in $D_{10–15}$ in June, and −0.44°C ± 1.53°C in $D_{15–50}$ in October. The monthly T_{me} in $D_{15–50}$ is positive throughout most of the year, even in November and December, which means that heat diffuses to sufficient depths (Fig. 5d). The negative bias in autumn could be the result of insufficient deepening of the thermocline at the beginning of destratification. Also, as indicated by the values of N^2 shown in Fig. 9c, the strength of stratification is well simulated over this 10-yr period, and the deepening of M_{LB} agrees with observations (Fig. 8c), even during strong stratification periods. Seasonal variations of water temperature in $D_{50–100}$ are also well captured (Fig. 5e).

FLake—This model simulates water temperature profiles that produce high T_{rmse} (between 2°C and 4°C) very rapidly. During the water warming period, a maximum monthly T_{me} negative in $D_{0–5}$ (−2.67°C ± 1.82°C in June)

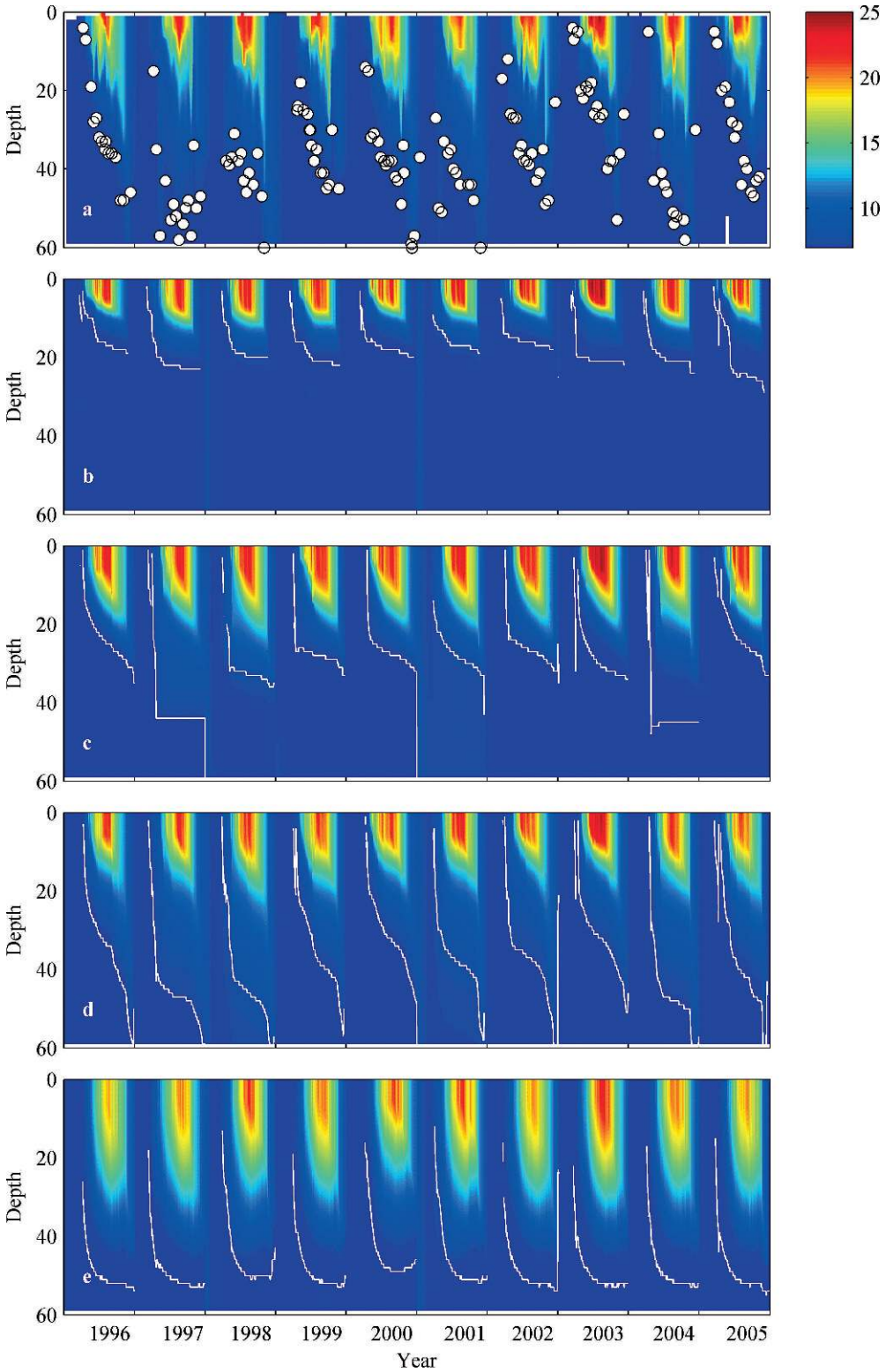

Fig. 8. Temperature contour plots of (a) the interpolated observed data and of simulated data with (b) HLM, (c) DYRESM, (d) SIMSTRAT, and (e) FLake, from 01 January 1996 to 31 December 2005. The observed M_{LB} and the M_{LB} of each model are indicated in white from 01 May to 31 October of years 1996–2005.

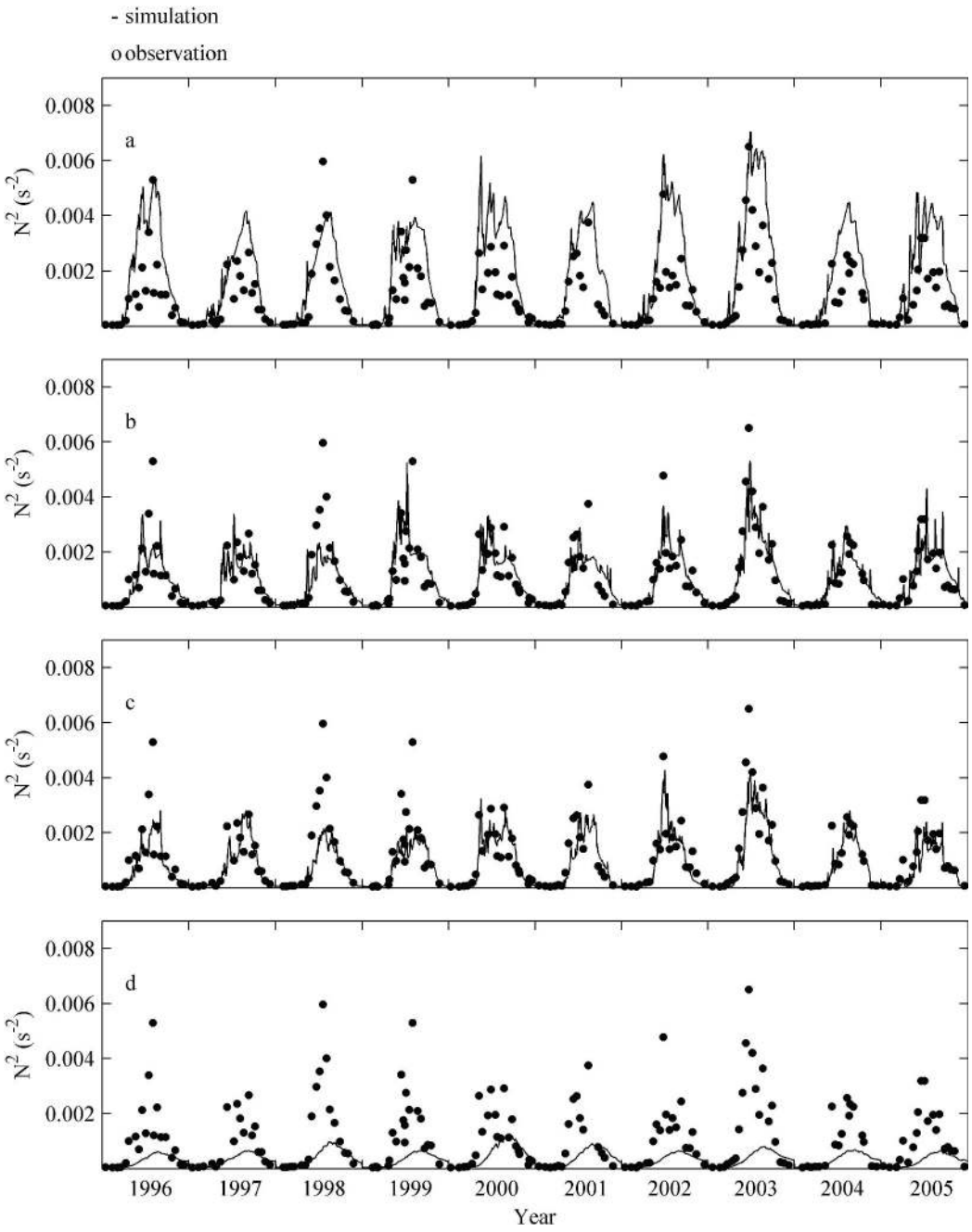

Fig. 9. Index of stratification N^2 from 01 January 1996 to 31 December 2005 for the observed data and for data simulated with (a) HLM, (b) DYRESM, (c) SIMSTRAT, and (d) FLake.

is predicted, whereas during the destratification period, maximum monthly T_{me} in D_{0-5} (2.27°C ± 0.75°C in November) and D_{5-10} (2.46°C ± 1.14°C in October) are positive. This emphasizes a significant lag in the temporal evolution of the simulated temperature (Fig. 6a,b). During the same periods (as shown in Fig. 6d), temperatures in the deeper layers were overestimated (monthly T_{me} between 0.42°C ± 1.29°C and 2.56°C ± 2.38°C in D_{15-50}). This trend is the result of the formation of a thermocline too thick in spring that, instead of being steepest in the topmost layers, declines monotonically to the bottom and prevents accurate development of the thermocline later in the year. Therefore M_{LB} develops at greater depth than observed (Fig. 8d), and the slope of the thermocline is less abrupt, explaining the high T_{rmse} through the profile and smaller values of N^2 (Fig. 9d). Because of the virtual bottom of the lake set at 60 m, heat loss was enhanced during non-stratified periods.

Additional assessments—The date of first occurrence of M_{LB} (O_T) was diagnosed each year for both the simulations and observations. Because temperature soundings have not

been made with the same frequency as those of the model water temperature archives, O_T is diagnosed when the thermocline is well established in the observed profiles. It is difficult to have accurate estimates of O_T because of the sparsity of the soundings (every 2 weeks), since the thermocline can develop any time between one sounding and the next. Nevertheless, it seems that the O_T simulated by DYRESM, SIMSTRAT, and FLake are quite similar and appear either in one sounding or in the time that elapsed between two soundings. In HLM, stratification always appeared earlier than the other models, but between the same two soundings, with three exceptions.

Finally, for a set of 182 observed and simulated surface water temperatures (0.4 m), the correlation coefficients are $r > 0.98$ for HLM, DYRESM, and SIMSTRAT and 0.91 for FLake. Annual T_{me} are $-0.1°C \pm 1.1°C$, $0.27°C \pm 1.14°C$, and $-0.44°C \pm 0.99°C$ for HLM, DYRESM, and SIMSTRAT, respectively. Overall, FLake produces lower surface temperatures, with a T_{me} of $-0.84°C \pm 2.4°C$.

Discussion

The main goal of this study was to evaluate the suitability of one-dimensional lake models to reproduce the evolution of water temperature profiles in the deep perialpine Lake Geneva. Despite controversy regarding the application of one-dimensional models to large and deep lakes, particularly because atmospheric conditions are heterogeneous over extensive water surface areas, and because horizontal advection is neglected in the lake and seiching motion is parameterized in a rather rudimentary way, we have nevertheless shown that some models, after slight calibration and with no significant changes to model formulations, are able to predict seasonal evolution of water temperature profiles with reasonable accuracy.

It has already been shown that for shallower lakes (e.g., Pyramid Lake [100 m], Yellowstone Lake [98 m], and Sparkling Lake [20 m] in the United States), HLM and FLake accurately predicted temperature profiles (Hostetler and Bartlein 1990; Hostetler and Giorgi 1995; A. Martynov unpubl.). However, at Lake Geneva's deep station (SHL2), it appears that HLM and FLake limitations have been reached in terms of simulating thickness and seasonal deepening of the thermocline. Consequently, their temperature profiles are not well reproduced. On the one hand, the FLake model tends to generate too strong a mixing and the HLM simulates too weak a mixing, which consequently affects the timing and position of the thermocline. Because both momentum and heat are similarly exchanged at the air–lake interface, the discrepancies in the intensity of the mixing are probably due to internal structure and processes involved in each model. The onset of stratification, earlier in HLM than in the other models, is related to a thermocline that hardly deepens and with a largely underestimated M_{LB}. Once the threshold of maximum increase of the eddy-diffusion coefficient is reached, the values then level off with increasing wind speed. After inaccurate reproduction of the mixed-layer depth with a similar eddy diffusion model, McCormick and Meadows (1988) had already identified such a problem. It appears that the seiche parameterization is a missing fundamental process that should increase the actual value of eddy-diffusion coefficients in highly stratified layers and improve the prediction of heat penetration in deeper layers. To explain the disagreements between observations and FLake simulations, one should remember that physical processes, such as heat diffusion, are not explicitly evoked in this model; instead, they are based on self-similarity concepts of the temperature–depth curve. However, the virtual bottom of the FLake model might be the primary source of error and a limiting factor for application to lakes in which the annual variability is still important at 60 m depth. The model simulates excessive cooling in winter as heat lost is concentrated in a reduced volume that enables complete overturn. A good representation of the profiles during the cold period is essential, in that those produced before stratification determine the future evolution of the thermocline. Furthermore, the observed thermocline in spring often develops close to the surface with a steeper slope in shallow water. Such a curve cannot be reproduced in FLake because the thermocline is located between the lower limit of the mixed layer and the bottom of the lake. This definition of the thermocline might, on such occasions, be detrimental to development of future temperature profiles. On the other hand, the surface temperature predictions of HLM, with an annual T_{me} on the order of $-0.1°C \pm 1.1°C$ and in $D_{0–5}$ of $0.08°C \pm 1.25°C$, are remarkable.

This model intercomparison shows that DYRESM and SIMSTRAT are capable of reproducing multiple aspects of the evolution of water temperature profiles at Sta. SHL2. The best agreement between predicted and observed data is at the surface and in $D_{0–5}$. Accurate results are also found in layers between 5 and 50 m, with slightly better agreement for SIMSTRAT. The main challenge for the models lies in the $D_{5–10}$ and the $D_{10–15}$ layers to correctly simulate the location and the slope of the seasonal thermocline. Even minor disagreements in the deepening of the thermocline in summer can generate large T_{rmse}. Compared with HLM and FLake, both DYRESM and SIMSTRAT have the advantage of parameterizing certain three-dimensional processes, such as seiching effects on mixing, and might explain the accurate prediction of the simulated profiles. Nevertheless, because of the intrinsic inability of one-dimensional models to reproduce physically all processes in lakes, displacements of the thermocline during such seiching events are not accurately resolved. Soundings taken during or soon after those events could increase the temperature variability, thereby affecting T_{rmse}. Because of the poor temporal resolution of the water temperature soundings, pronounced thermocline displacements are, however, rarely observed, and systematic offsets cannot be identified. However, although T_{rmse} of both the DYRESM and SIMSTRAT models reproduced similar temperature profiles from quasi-vertical isothermal conditions until the beginning of summer, SIMSTRAT performed better (Fig. 7g–i) during the period of strongest stratification ($<2°C$ for SIMSTRAT and $<3°C$ for DYRESM in $D_{5–10}$ and $D_{10–15}$).

Overestimation of temperature in $D_{5–15}$ and its underestimation below, as well as the lack of seasonal variability of

the M_{LB} simulated by DYRESM, indicate insufficient heat below the thermocline. Similar hypolimnion temperature predictions were simulated in a number of lakes with a combination of hypotheses to explain those differences, primarily ensuing from field data or model structure (Romero and Melack 1996; Rutherford et al. 1996; Copetti et al. 2006). As also shown by Tanentzap et al. (2007), the calibration does not enable one to identify a particular mixing parameter that would systematically reduce the error. The enhanced surface mixed-layer algorithm and the new deep-mixing algorithms implemented in DYRESM improved predictions of the thermal structure of various lakes (Yeates and Imberger 2003). Additionally, the new version has reduced disagreement between observed and simulated data in the hypolimnia of some of those lakes (Gal et al. 2003; Yeates and Imberger 2003). However, the underestimated variability of temperatures exhibited in the lower metalimnion and hypolimnion show that the parameterization of internal mixing might not yet be appropriate for Lake Geneva. Despite a similar 240 m depth, simulation with DYRESM over Lake Ontario produced lower surface temperature and a deeper thermocline (Boyce et al. 1993). It is difficult to assume in this study that the constant K_e is responsible for the temperature errors throughout the year and water depth (Gal et al. 2003; Tanentzap et al. 2007). Although the sensitivity analysis did not affect the performance of the model, temporal agreement between profiles differed depending on the value of K_e. This result emphasizes the need to account for seasonal effects of light penetration induced by changing phytoplankton populations.

Because of higher heat diffusion in the $D_{15–50}$ and $D_{50–100}$ layers, SIMSTRAT is the only model that significantly accounts for seasonal deep hypolimnion temperature variations. Despite the accurate correlation in the upper layers, the smoothed hypolimnetic seasonal temperature cycles predicted by DYRESM could cause an issue over multiyear simulations. Insufficient heat storage with depth might increase discrepancies in the water column over the years and eventually change the extent of the dynamic processes, in that the lake does not overturn regularly, and so temperature through the column might not be homogenized each winter.

It has been shown above that a one-dimensional lake model can be used to simulate thermal profiles at SHL2, providing some adjustments are made that influence heat diffusion. The sensitivity of the models to variable or wind speed–dependent c_D has been tested, and lower T_{rmse} between observed and simulated profiles are found when c_D is higher than the constant default value or accounts for wind speed. Similarly, a seiching parameterization reduces the T_{rmse} because heat diffusion does not cease in highly stratified layers. Scaling of the wind speed at the land station has proven beneficial for simulation of the thermal profile because it better represents conditions over the lake at Sta. SHL2.

This is the first time that several one-dimensional models, with common external driving variables and common heat flux parameterizations, have been compared to assess their capacity to reproduce temperature profiles in the deep domain of Lake Geneva (Sta. SHL2). Owing to inclusion of detailed physics, SIMSTRAT and DYRESM perform better at this particular location. Based on these rather encouraging results, the use of lake models to investigate other aspects of Lake Geneva in a changing climate clearly becomes possible. Issues that need to be addressed concern the temperature increases related to enhanced atmospheric CO_2 concentrations over a much longer period than that investigated here, in which the thermal response of the lake will be investigated numerically in terms of the amount of heat stored over a century timescale. Initial experiments conducted on deep Swiss lakes have shown the significant effect of a temperature increase on the entire column and the need to use a continuous modeling approach for lakes that do not freeze each year. Typically, heat is stored in the hypolimnion and accumulates year after year (Peeters et al. 2002) within lakes, which are rarely dimictic, especially those that are deep.

If, as shown in this paper, models are capable of adequately simulating the timing of the onset of stratification, the thickness of the metalimnion, and the maximum stability of the thermocline, then there is room for further studies involving, for example, coupled physical and biological models. Such coupled model experiments can help understand changes in biogeochemical processes under shifting conditions of lake temperature and stratification. Such changes could have an effect on the proliferation of toxic algae and other aquatic pathogens that could ultimately result in a reduction of water quality and possibly to problems of public health. However, even though DYRESM and SIMSTRAT have shown genuine skill in simulating temperature profiles down to deep layers, the lake model required for biological applications needs to perform accurately through the whole water column, in that it could affect the performance of coupled biochemical models. DYRESM discrepancies in the bottom layer might not only potentially neglect interannual temperature variations, but also alter the biological and chemical properties in the upper layers. Furthermore, one should keep in mind that the models presented here do not consider all mixing processes observed in the lakes, and limits might therefore be reached. The Rhone River underflows (Loizeau and Dominik 2000) or cascades of cold water from rapid cooling of the shallow Petit Lac or shallow lake areas in winter (Fer et al. 2002) are, for instance, not considered. By omitting deep winter convection related to these intrusions, oxygen supply to the deep water could be underestimated and phosphorus release overestimated, with effects on biogeochemical processes. The results presented in this paper suggest that models today can be used for applications beyond investigations solely of physical processes; they are now in a position to attempt effects-oriented modeling for issues such as water quality in a changing climate.

Acknowledgments

We are grateful to S. W. Hostetler from the U.S. Geological Survey, the Centre for Water Research (CWR), and the Swiss Federal Institute of Aquatic Science and Technology (EAWAG) and in particular to M. Schmidt and D. Mironov from the German Weather Service (DWD) for providing us the lake models and technical support. We are thankful to the French "Station d'Hydrobiologie Lacustre" of Lake Geneva (managed by the

French National Institute for Agricultural Research, INRA) for collecting water temperature profiles at Sta. SHL2 over the period 1996–2005 and for making these available for the purposes of this study. We would like to thank particularly S. Jacquet for his scientific remarks and advice and his efforts to make the collaboration possible between our two institutes. We also thank the reviewers for their helpful suggestions made on this manuscript. Their comments were particularly valuable and enhanced the quality of the text.

References

Anneville, O., S. Souissi, S. Gammeter, and D. Straile. 2004. Seasonal and inter-annual scales of variability in phytoplankton assemblages: comparaison of phytoplankton dynamics in three peri-alpine lakes over a period of 28 years. Freshw. Biol. **49:** 98–115.

———, ———, F. Ibanez, V. Ginot, J. C. Druart, and N. Angeli. 2002. Temporal mapping of phytoplankton assemblages in Lake Geneva: Annual and interannual changes in their patterns of succession. Limnol. Oceanogr. **47:** 1355–1366.

Bantle, H. 1989. Program documentation for climatic-database at RZ-ETH Zürich. MeteoSwiss Publication. [In German.]

Bettems, J. M. 2002. EUCOS impact study using the limited-area non-hydrostatic NWP model in operational use at Meteo-Swiss. COSMO, Tech. Rep. 5.

Bonan, G. D. 1996. A land surface model (LSM version 1.0) for ecological, hydrological, and atmospheric studies. Technical description and user's guide. NCAR Technical Note NCAR/TN-417 + STR, National Center for Atmospheric Research.

Boyce, F. M., P. F. Hamblin, L. D. Harvey, W. M. Schertzer, and R. C. McCrimmon. 1993. Response of the thermal structure of Lake Ontario to deep cooling water withdrawals and to global warming. J. Gt. Lakes Res. **19:** 603–616.

Bradley, E., P. Coppin, and J. Godfrey. 1991. Measurements of sensible and latent heat flux in the western equatorial Pacific ocean. J. Geophys. Res. **96:** 3375–3389.

Bührer, H., and H. Ambühl. 1975. The discharge of treated waste water into lakes. Schweiz. Z. Hydrol. **37:** 347–369. [In German.]

Burchard, H., and H. Baumert. 1995. On the performance of a mixed layer model based on the k–ε turbulence closure. J. Geophys. Res. **100:** 8523–8540.

———, O. Petersen, and T. P. Rippeth. 1998. Comparing the performance of the Mellor–Yamada and the κ–ε two-equation turbulence models. J. Geophys. Res. **103:** 10543–10554.

Capblancq, J. 1995. Autotroph primary production, *In* R. Pourriot and M. Meybeck [eds.], General limnology. Masson, [In French.]

Charnock, H. 1955. Wind stress on a water surface. Q. J. R. Meteorol. Soc. **81:** 639–640.

Copetti, D., G. Tartari, G. Morabito, A. Oggioni, E. Legnani, and J. Imberger. 2006. A biogeochemical model of lake Pusiano (North Italy) and its use in the predictability of phytoplankton blooms: First preliminary results. J. Limnol. **65:** 59–64.

Dake, J. M. K., and D. R. F. Harleman. 1969. Thermal stratification in lakes—analytical and laboratory studies. Water Resour. Res. **5:** 484–495.

Fer, I., U. Lemmin, and S. A. Thorpe. 2002. Winter cascading of cold water in Lake Geneva. J. Geophys. Res. **107:** 2236–2569.

Gal, G., J. Imberger, T. Zohary, J. Antenucci, A. Anis, and T. Rosenberg. 2003. Simulating the thermal dynamics of Lake Kinneret. Ecol. Model. **162:** 69–86.

Geernaert, G. L., S. E. Larsen, and F. Hansen. 1987. Measurements of the wind stress, heat flux, and turbulence intensity during storm conditions over the North Sea. J. Geophys. Res. **92:** 13127–13139.

Gerten, D., and R. Adrian. 2000. Climate-driven changes in spring phytoplankton dynamics and the sensitivity of shallow polymictic lakes to the North Atlantic Oscillation. Limnol. Oceanogr. **45:** 1058–1066.

Goudsmit, G-H., H. Burchard, F. Peeters, and A. Wüest. 2002. Application of k–ε turbulence models to enclosed basins: The role of internal seiches. J. Geophys. Res. **107:** 3230–3243, doi:10.1029/2001JC000954.

Graf, W. H., N. Merzi, and C. Perrinjaquet. 1984. Aerodynamic drag: Measured at a nearshore platform on Lake Geneva. Arch. Meteor. Geophys. Bioclim. **33:** 151–173.

Hamilton, D. P., and S. G. Schladow. 1997. Prediction of water quality in lakes and reservoirs: Part I—model description. Ecol. Model. **96:** 91–110, doi: 10.1016/S0304-3800(96)00062-2.

Henderson-Sellers, B. 1985. New formulation of eddy diffusion thermocline models. Appl. Math. Model. **9:** 441–446.

———. 1986. Calculating the surface energy balance for lake and reservoir modeling: A review. Rev. Geophys. **24:** 625–649.

———, M. J. McCormick, and D. Scavia. 1983. A comparison of the formulation for eddy diffusion in two one-dimensional stratification models. Appl. Math. Model. **7:** 212–215.

Hornung, R. 2002. Numerical modelling of stratification in Lake Constance with the 1-D hydrodynamic model DYRESM. M.S. thesis. Univ. of Stuttgart, Germany.

Hostetler, S. W. 1987. Simulation of lake evaporation with an energy balance-eddy diffusion model of lake temperature: Model development and validation, and application to lake-level variations at Harney–Malheur Lake. Ph.D. thesis. Univ. of Oregon.

———, and P. J. Bartlein. 1990. Simulation of lake evaporation with application to modelling lake-level variations at Harney–Malheur Lake, Oregon, Water Resour. Res. **26:** 2603–2612.

———, and F. Giorgi. 1995. Effects of a $2 \times CO_2$ climate on two large lake systems: Pyramid Lake, Nevada, and Yellowstone Lake, Wyoming. Glob. Planet. Change **10:** 43–54.

Imberger, J., and J. C. Patterson. 1981. A dynamic reservoir simulation model: DYRESM5, p. 310–361. *In* H. B. Fischer [ed.], Transport models for inland and coastal waters. Academic Press.

———, ———, B. Hebbert, and I. Loh. 1978. Dynamics of reservoir of medium size. J. Fluid Mech. **78:** 489–512.

Jacquet, S., and others. 2005. The proliferation of the toxic cyanobacterium *Planktothrix rubescens* following restoration of the largest natural French lake (Lake Bourget). Harmful Algae **4:** 651–672.

Jöhnk, K., J. Huisman, J. Sharples, B. Sommeijer, P. Visser, and J. Stroom. 2008. Summer heatwaves promote blooms of harmful cyanobacteria. Glob. Change Biol. **14:** 495–512.

King, J. R., B. J. Shuter, and A. P. Zimmerman. 1997. The response of the thermal stratification of South Bay (Lake Huron) to climatic variability. Can. J. Fish. Aquat. Sci. **54:** 1873–1882.

Kitaigorodskii, S. A., and Y. Z. Miropolsky. 1970. On the theory of the open ocean active layer. Izv. Akad. Nauk SSSR Fizika Atmosfery i Okeana **6:** 178–188.

Kraus, E. B., and J. S. Turner. 1967. A one dimensional model of the seasonal thermocline: II. The general theory of its consequences. Tellus **19:** 98–106.

Lazzarotto, J., P. Nirel, F. Rapin. 2006. Physical-chemical changes in the waters of Lake Geneva, p. 31–63. *In* CIPEL [eds.], Report of the international commission for the protection of the waters of lake Geneva against pollution, Campaign 2005. [In French.]

———, F. Rapin. 2007. Physical-chemical changes in the waters of Lake Geneva, p. 33–57. *In* CIPEL [eds.], Report of the international commission for the protection of the waters of lake Geneva against pollution, Campaign 2006. [In French.]

Legnani, E., D. Copetti, A. Oggioni, G. Tartari, M. T. Palumbo, and G. Morabito. 2005. Planktothrix rubescens'-seasonal dynamics and vertical distribution in Lake Pusiano (North Italy). J. Limnol. **64:** 61–73.

Lemmin, U., and N. D'Adamo. 1996. Summertime winds and direct cyclonic circulation: Observations from Lake Geneva. Ann. Geophys. **14:** 1207–1220.

Lin, W., L. P. Sanford, S. E. Suttles, and R. A. Valigura. 2002. Drag coefficients with fetch limited wind waves. J. Phys. Oceanogr. **32:** 3058–3074.

Loizeau, J-L., and J. Dominik. 2000. Evolution of the Rhone river discharge during the last 80 years and some implications for Lake Geneva. Aquat. Sci. **62:** 54–67.

McCormick, M. J., and G. L. Fahnenstiel. 1999. Recent climatic trends in nearshore water temperatures in the St. Lawrence Great Lakes. Limnol. Oceanogr. **44:** 530–540.

———, and G. A. Meadows. 1988. An intercomparison of four mixed layer models in a shallow inland sea. J. Geophy. Res. **93:** 6774–6788.

Mironov, D. V. 2008. Parameterization of lakes in numerical weather prediction. Description of a lake model. Deutscher Wetterdienst, COSMO Tech. Rep. 11.

Orlob, G. T., and L. G. Selna. 1970. Temperature variations in deep reservoirs. J. Hydraul. Div. Proc. **96:** 393–410.

Peeters, F., D. M. Livingstone, G. Goudsmit, R. Kipfer, and R. Forster. 2002. Modeling 50 years of historical temperature profiles in a large central European lake. Limnol. Oceanogr. **47:** 186–197.

———, D. Straile, A. Lorke, and D. M. Livingstone. 2007. Earlier onset of the spring phytoplankton bloom in lakes of the temperate zone in a warmer climate. Glob. Change Biol. **13:** 1898–1909.

Richards, J. M. 1971. Simple expressions for the saturation vapor pressure of water in the range −50 to 140°C. Br. J. Appl. Phys. **4:** L15–L18.

Rodi, W. 1984. Turbulence models and their application in hydrodynamics—a state of the art review, 2nd ed. Int. Assoc. Hydraul. Res.

Romero, J. R., and J. M. Melack. 1996. Sensitivity of vertical mixing in a large saline lake to variations in runoff. Limnol. Oceanogr. **41:** 955–965.

Rutherford, J. C., S. M. Dumnov, and A. H. Ross. 1996. Predictions of phosphorus in Lake Rotorua following load reductions. N. Z. J. Mar. Freshw. Res. **30:** 383–396.

SAEFL, Swiss Agency for the Environment, Forests and Landscape. 1994. The state of lakes in Switzerland. Cahier de l'environnement 237. [In French.]

Shatwell, T., J. Köhler, and A. Nicklisch. 2008. Warming promotes cold-adapted phytoplankton in temperate lakes and opens a loophole for Oscillatoriales in spring. Glob. Change Biol. **14:** 1–7.

Smith, S. D., and others. 1992. Sea surface wind stress and drag coefficients: the HEXOS results. Bound. Layer Meteorol. **60:** 109–142.

Straile, D., D. M. Livingstone, G. A. Weyhenmeyer, and D. G. George. 2003. The response of freshwater ecosystems to climate variability associated with the North Atlantic Oscillation, p. 263–279. *In* J. W. Hurrell, Y. Kushnir, G. Ottersen and M. Visbeck [eds.], The North Atlantic Oscillation: Climatic significance and environmental impact. AGU Geophysical Monograph Series 134.

SVGW. 2008. Swiss company of water and gas industry. Information on drinking water. TWI 12. [In German.]

Tanentzap, A. J., D. P. Hamilton, and N. D. Yan. 2007. Calibrating the dynamic reservoir simulation model (DYRESM) and filling required data gaps for 1-dimensional thermal profile predictions in a boreal lake. Limnol. Oceanogr. Methods **5:** 484–494.

Umlauf, L., and U. Lemmin. 2005. Interbasin exchange and mixing in the hypolimnion of a large lake: The role of long internal waves. Limnol. Oceanogr. **50:** 1601–1611.

UNESCO. 1981. The practical salinity scale 1978 and the international equation of state of seawater 1980. Tenth Report of the Joint Panel on Oceanographic Tables and Standards. Division of Marine Sciences Tech. Pap. in Mar. Sci. UNESCO.

Walsby, A. E., and F. Schanz. 2002. Light-dependent growth rate determines changes in the population of *Planktothrix rubescens* over the annual cycle in Lake Zürich, Switzerland. New Phytol. **154:** 671–687.

Wüest, A., and A. Lorke. 2003. Small-scale hydrodynamics in lakes. Annu. Rev. Fluid Mech. **35:** 373–412.

———, G. Piepke, and J. D. Halfman. 1996. Combined effects of dissolved solids and temperature on the density stratification of Lake Malawi, p. 183–202. *In* T. C. Johnson and E. O. Oada [eds.], The limnology, climatology and paleoclimatology of the East African Lakes. Gordon and Breach.

Yeates, P. S., and J. Imberger. 2003. Pseudo two-dimensional simulations of internal and boundary fluxes in stratified lakes and reservoirs. Int. J. River Basin Manag. **1:** 279–319.

Associate editor: Peter A. Jumars

Received: 09 December 2008
Accepted: 14 April 2009
Amended: 05 May 2009